AMP-activated protein kinase and adenylate kinase prevent the ATP catastrophe and cytotoxic protein aggregation

Masak Takaine[1,2]*, Hiromi Imamura[3], Satoshi Yoshida[1,2,4,5]*

[1]Gunma University Initiative for Advanced Research (GIAR), Gunma University, Maebashi 371-8512, Japan
[2]Institute for Molecular and Cellular Regulation (IMCR), Gunma University, Maebashi 371-8512, Japan
[3]Graduate School of Biostudies, Kyoto University, Kyoto 606-8501, Japan
[4]School of International Liberal Studies, Waseda University, Tokyo, 169-8050, Japan
[5]Japan Science and Technology Agency, PREST

*Correspondence should be addressed to: masaktakaine@gunma-u.ac.jp (M.T.) (Lead contact) or satosh@waseda.jp (S.Y.)

Running title

ATP homeostasis prevents cytotoxic protein aggregation

Keywords

ATP, homeostasis, proteostasis, yeast, neurodegenerative disease, AMPK, protein aggregation

ABSTRACT

ATP is the main source of chemical energy in all life and is maintained at several millimolar in eukaryotic cells. However, the mechanisms responsible for and physiological relevance of this high and stable concentration of ATP remain unclear. We herein demonstrate that AMP-activated protein kinase (AMPK) and adenylate kinase (ADK) cooperate to maintain cellular ATP levels regardless of glucose concentrations. Single cell imaging of ATP-reduced yeast mutants revealed that ATP concentrations in these mutants underwent stochastic and transient depletion of ATP repeatedly, which induced the cytotoxic aggregation of endogenous proteins and pathogenic proteins, such as huntingtin and α-synuclein. Moreover, pharmacological elevations in ATP levels in an ATP-reduced mutant prevented the accumulation of α-synuclein aggregates and its cytotoxicity. The removal of cytotoxic aggregates depended on proteasomes, and proteasomal activity cooperated with AMPK or ADK to resist proteotoxic stresses. The present results provide the first evidence to show that cellular ATP homeostasis ensures proteostasis and revealed that stochastic fluctuations in cellular ATP concentrations contribute to cytotoxic protein aggregation, implying that AMPK and ADK are important factors that prevent proteinopathies, such as neurodegenerative diseases.

INTRODUCTION

Adenosine triphosphate (ATP) is the main energy currency used by all living organisms. Due to high demand, the turnover rate of ATP is estimated to be less than one minute in yeast and metazoans (Mortensen, Thaning et al., 2011, Takaine, Ueno et al., 2019). In addition to its role as energy currency, recent studies reported that ATP may influence the balance between the soluble and aggregated states of proteins, suggesting that proteostasis is maintained by energy-dependent chaperones and also by the property of ATP as a hydrotrope to solubilize proteins (Hayes, Peuchen et al., 2018, Patel, Malinovska et al., 2017). Recent proteomic analyses demonstrated that many cellular proteins are insoluble at submillimolar ATP concentrations and become soluble at ATP concentrations > 2 mM (Sridharan, Kurzawa et al., 2019); however, it currently remains unclear whether ATP-dependent protein solubilization/desolubilization play any significant roles in cell physiology.

We recently established a reliable imaging technique to quantify intracellular ATP concentrations in single living yeast cells using the genetically encoded fluorescent ATP biosensor QUEEN (Yaginuma, Kawai et al., 2014), which enables long-term evaluations of ATP homeostasis in individual cells (Takaine et al., 2019). Our findings demonstrated that intracellular ATP concentrations did not vary within a yeast population grown in the same culture (Takaine et al., 2019), which was in contrast to the large variations observed in intracellular ATP concentrations within a bacterial cell population (Yaginuma et al., 2014). Moreover, intracellular ATP concentrations in individual living yeast cells were stably and robustly maintained at approximately 4 mM, irrespective of carbon sources and cell cycle stages, and temporal fluctuations in intracellular ATP concentrations were small (Takaine et al., 2019). Based on these findings, we hypothesized that an exceptionally robust mechanism may exist to precisely regulate ATP concentrations in eukaryotes. It also remains unclear why ATP is stably maintained at a markedly higher concentration than the K_m (Michaelis constant) required for the enzymatic activity of almost all ATPases (Edelman, Blumenthal et al., 1987), and the consequences associated with failed ATP homeostasis in living organisms have not yet been elucidated.

The most promising candidate regulator of ATP homeostasis is AMP-activated protein kinase (AMPK). AMPK, which is activated by AMP and inhibited by ATP (Xiao, Heath et al., 2007), has long been regarded as an important regulator of the whole-body and cellular energy status in eukaryotes (Hardie, Schaffer et al., 2016). AMPK is activated by increases in the AMP:ATP or ADP:ATP ratio (*i.e.,* low-energy state), and regulates its downstream effectors

76 by phosphorylation to redirect cell metabolism from an anabolic (ATP-consuming) state to
77 catabolic (ATP-producing) state (Herzig & Shaw, 2017). In the budding yeast *Saccharomyces*
78 *cerevisiae*, the sucrose non-fermenting 1 (Snf1) protein kinase complex is the sole AMPK.
79 Similar to other AMPKs, the yeast Snf1 complex comprises three subunits: the catalytic α
80 subunit (*SNF1*), scaffolding β subunit (*SIP1*, *SIP2* or *GAL83*), and regulatory γ subunit
81 (*SNF4*) (Ghillebert, Swinnen et al., 2011). The role of the Snf1 complex in adaptation to
82 glucose limitations has been characterized in detail (Hedbacker & Carlson, 2008). In the
83 presence of sufficient glucose in the medium, the Snf1 complex is inactive (Wilson, Hawley
84 et al., 1996). When glucose concentrations decrease, the Snf1 complex is activated and
85 phosphorylates the transcriptional repressor Mig1, which then triggers the transcription of
86 numerous glucose-repressed genes (Carlson, 1999). However, the contribution of AMPK or
87 the Snf1 complex to cellular ATP levels remains unknown.
88
89 Other possible candidate regulators of ATP homeostasis include genes whose mutation leads
90 to decreases in the cellular content of ATP. However, based on biochemical analyses of cell
91 populations, few yeast mutants reduced ATP levels (Gauthier, Coulpier et al., 2008,
92 Ljungdahl & Daignan-Fornier, 2012). Adenylate kinase (ADK) is a key enzyme that
93 synthesizes ATP and AMP using two ADP molecules as substrates, and the null-mutant of
94 ADK (*adk1*Δ) was shown to have a reduced cellular ATP concentration (~70% of the wild
95 type) (Gauthier et al., 2008). Bas1 is a transcription factor that is required for *de novo* purine
96 synthesis and *bas1*Δ has also a reduced ATP concentration (~50% of the wild type) (Gauthier
97 et al., 2008). However, the regulation of ATP concentrations and the physiological
98 consequences of reduced ATP levels in these mutants remain unclear, particularly at the
99 single cell level.
100
101 In the present study, we investigated the roles of AMPK, ADK, and Bas1 in ATP homeostasis
102 using the QUEEN-based single cell ATP imaging technique. We demonstrated for the first
103 time that AMPK is involved in the regulation of intracellular ATP concentrations, even under
104 glucose-rich conditions. Furthermore, time-lapse ATP imaging revealed that cells lacking
105 both AMPK and ADK frequently underwent transient ATP depletion, while ATP
106 concentrations oscillated in those lacking Bas1. These ATP dynamics in the mutants were
107 overlooked in previous biochemical studies. We found that some intrinsic proteins and
108 aggregation-prone model proteins, including α-synuclein, which is responsible for Parkinson's
109 disease, aggregated and were cytotoxic in all of the ATP-reduced mutants tested. The present
110 results suggest that the stable maintenance of ATP is essential for proteostasis and imply that

111 an ATP crisis promotes proteinopathies, such as neurodegenerative diseases.

112 **RESULTS**

113 AMPK is involved in the maintenance of cellular ATP levels

114 We recently developed a reliable monitoring system for cytoplasmic ATP concentrations in
115 living yeast cells using the ATP biosensor QUEEN (Takaine et al., 2019). We conducted a
116 more detailed examination of ATP dynamics in wild-type and mutant yeast cells using this
117 system in the present study. We investigated whether the deletion of *SNF1*, which encodes a
118 catalytic subunit of AMPK, affects cellular ATP concentrations. In *SNF1*-null mutant (*snf1*Δ)
119 cells, cellular ATP levels were significantly lower than those in wild-type cells at all glucose
120 concentrations tested (2, 0.2, and 0.05%) (Fig. 1A, B). It is important to note that even under
121 high glucose conditions (2% glucose), in which the Snf1 complex is considered to be inactive,
122 *snf1*Δ cells showed significantly reduced ATP levels. Moreover, the deletion of each gene
123 encoding the β subunit of AMPK (*SIP1*, *SIP2*, or *GAL83*) reduced cellular ATP levels to a
124 similar extent as the deletion of *SNF1*, suggesting that three subtypes of the Snf1 complex are
125 involved in maintaining ATP concentrations (Fig. 1C). On the other hand, the deletion of
126 *MIG1*, which encodes a major downstream target of the Snf1 complex in glucose repression,
127 had a negligible effect on ATP levels (Fig. 1D), suggesting that unknown factors other than
128 Mig1 primarily regulate ATP levels under the control of the Snf1 complex. Collectively, these
129 results demonstrated for the first time that AMPK/SNF1 affect cellular ATP concentrations
130 even under glucose-rich conditions.

131

132 Adenylate kinase ADK1 cooperates with AMPK to regulate ATP homeostasis

133 Adenylate kinase catalyzes the interconversion of adenine nucleotides (ATP+AMP ⟷
134 2ADP), which is important for *de novo* adenine nucleotide synthesis and the balance of ATP,
135 ADP, and AMP. Previous biochemical studies reported that the deletion of the adenylate
136 kinase gene reduced ATP concentrations in mouse skeletal muscle cells and budding yeasts
137 (Gauthier et al., 2008, Janssen, Dzeja et al., 2000). We confirmed these findings using an
138 ATP imaging method: *adk1*Δ cells showed significantly lower QUEEN ratios than wild-type
139 cells on average in the presence of sufficient carbon sources (Fig. S1).

140

141 In addition to being a key enzyme in purine metabolism, adenylate kinase has also been
142 suggested to cooperate with AMPK in order to monitor the cellular energy state (Hardie,
143 Carling et al., 1998). Therefore, we compared ATP levels in *snf1*Δ *adk1*Δ double mutant cells
144 with those in *snf1*Δ, *adk1*Δ, and wild-type cells (Fig. 2A, B). The data obtained were
145 represented by a dot plot that shows distribution characteristics in extensive detail. *snf1Δ*
146 *adk1Δ* cells had significantly lower average ATP levels than single mutant cells. We also

147 found not only a general reduction, but also a huge variation in ATP levels in the *snf1*Δ,
148 *adk1Δ, snf1*Δ *adk1Δ* cell population, as indicated by the large coefficient of variance (CV)
149 (Fig. 2B). Furthermore, some cells had extremely low ATP levels in *snf1Δ adk1Δ* (Fig. 2A,
150 B). These results suggest that Adk1 and the Snf1 complex both synergistically contribute to
151 ATP homeostasis.
152

153 ## A large pool of adenine nucleotide is important for maintaining cellular ATP
154 concentrations

155 We also examined a *bas1Δ* mutant, which is defective in the expression of genes responsible
156 for adenine biogenesis (Daignan-Fornier & Fink, 1992, Denis, Boucherie et al., 1998).
157 Consistent with previous biochemical findings (Gauthier et al., 2008), ATP levels quantified
158 by QUEEN were reduced by ~50% in *bas1Δ* cells (Fig. 2C, D). We found not only a general
159 reduction, but also a large variation in ATP levels in the *bas1Δ* cell population, as indicated
160 by the large CV (Fig. 2D). The decrease observed in ATP levels was due to reduced adenine
161 biosynthesis because the addition of extra adenine to media partially restored ATP levels (Fig.
162 2D). These results suggest that the sufficient production of adenine nucleotides is essential for
163 the stable maintenance of ATP levels. Moreover, the role of Bas1 in maintaining ATP levels
164 appeared to be epistatic to that of Snf1 because *bas1Δ snf1Δ* double mutant cells showed a
165 similar distribution of ATP levels to *bas1Δ* cells (Fig. S2).
166

167 ## ATP levels temporally fluctuate in ATP mutant cells

168 To investigate the mechanisms contributing to the large variations in ATP concentrations in
169 *snf1Δ adk1Δ* cells in more detail, we employed time-lapse ATP imaging (Fig. 3). We found
170 that the QUEEN ratio often underwent a rapid decline followed by recovery in *snf1Δ adk1Δ*
171 cells (see 116 and 132 min in Fig. 3A, C, and Movie S1, and 180 and 356 min in Fig. 3B, D,
172 and Movie S2). The sudden decrease in ATP concentrations (hereafter called "the ATP
173 catastrophe") occurred within a few minutes without any sign and was rarely observed in
174 wild-type cells (Takaine et al., 2019). The ATP catastrophe appeared to be a stochastic event
175 and cell intrinsic: these events occurred independent of cell cycle stages or cell sizes (compare
176 Fig. 3C with D). Under some conditions, the QUEEN ratio did not recover after the ATP
177 catastrophe and the cell died, as judged by the loss of QUEEN signals in the cell (Fig. S3).
178 These results suggest that the large variations in ATP concentrations observed in *snf1Δ adk1Δ*
179 cells were not simply due to a mixed population with different basal ATP levels, but were
180 rather due to the stochastic ATP catastrophe in individual cells.
181

182 Time-lapse imaging of *bas1Δ* revealed oscillatory cycles in ATP concentrations (Figs. 3E and
183 S4A, and Movies S3 and S4): ATP cycling in *bas1Δ* cells was slow (~35 min on average, Fig.
184 S4B) and distinguishable from that in *snf1Δ adk1Δ* cells; however, the common
185 characteristics of these mutants were that the concentration of ATP repeatedly reached close
186 to 0 mM. The ATP oscillation cycle was unsynchronized in the population and independent of
187 cell cycle progression, suggesting a unique metabolic rhythm intrinsic to each cell. The
188 oscillatory nature of ATP cycling in the *bas1Δ* mutant may involve a transcription/translation
189 cycle and will be described elsewhere.
190
191 ATP homeostasis is required for preventing protein aggregation.
192 We recently reported that cellular ATP concentrations are stably maintained at ~4 mM in
193 budding yeast (Takaine et al., 2019) and herein demonstrated that in the Snf1/AMPK complex,
194 Adk1 and Bas1 are required for the regulation of ATP homeostasis. However, the
195 physiological importance of ATP homeostasis remains unknown. To clarify the significance
196 of high ATP concentrations, we examined the global genetic interactions of *snf1Δ*, *adk1Δ*,
197 and *bas1Δ* using CellMap ((Usaj, Tan et al., 2017), thecellmap.org). An *in silico* analysis
198 identified genes involved in "protein folding/glycosylation" as common negative genetic
199 interactors with *adk1Δ* and *bas1Δ* (Fig. 4A). Negative genetic interactors of *ura6*, a gene
200 encoding uridylate kinase that also exhibits adenylate kinase activity, were enriched in the
201 "protein folding/glycosylation" category (Fig. 4A). We also found that interactors of *snf1*
202 were implicated in "protein folding/glycosylation. None of these mutants exhibited apparent
203 genetic interactions with genes in the "metabolism" category (Fig. 4A). The same analysis
204 using genetic and physical interactors provided similar results and showed that many
205 interactors were enriched in the "protein turnover" category (Fig. S5). These results imply that
206 although these three mutants regulate ATP with distinct mechanisms, all three have a
207 common cellular function.
208
209 To examine possible defects in protein folding and turnover (*i.e.*, proteostasis), we challenged
210 these mutants with various proteotoxic stresses. We found negligible growth defects in ATP
211 mutants under normal growth conditions with 2% glucose at 30°C (control in Fig. 4B),
212 suggesting that a high concentration of ATP is not necessary for cellular growth. However,
213 the *adk1* and *bas1* mutants both exhibited severe growth defects with a high temperature of
214 40°C, 1 hour of heat shock at 55°C, or in the presence of 0.5 μg/ml of the glycosylation
215 inhibitor tunicamycin or 2 mM H_2O_2. The *SNF1* deletion increased the stress sensitivity of
216 *adk1Δ* (Fig. 4B). This sensitivity to proteotoxic stress suggests that ATP homeostasis mutants

217 are defective in some aspects of proteostasis. We found that all four mutants tested contained
218 significantly increased numbers of Hsp104-GFP foci, a marker of protein aggregation
219 (Josefson, Andersson et al., 2017) (Fig. 4C, D). In contrast to Hsp104-GFP foci, Pab1-GFP, a
220 marker of stress granule (SG) assembly (Hoyle, Castelli et al., 2007), did not form foci in
221 ATP mutants, suggesting that protein aggregation and SG assembly are regulated in a distinct
222 manner (Fig. 4D). These analyses identified abnormal protein aggregation as a common
223 defect associated with ATP homeostasis mutants for the first time.
224

225 ## The transient depletion of ATP leads to the formation of protein aggregates

226 To examine whether ATP depletion triggers protein aggregation in living yeast, we artificially
227 depleted cellular ATP levels by replacing glucose with 2-deoxyglucose (2DG), a strong
228 inhibitor of glycolysis, in the media and monitored protein aggregation using Hsp104-GFP as
229 a marker of protein aggregation (Josefson et al., 2017) in wild-type cells. We previously
230 showed that ATP levels were almost completely depleted 2 minutes after the 2DG treatment
231 (Takaine et al., 2019). Within 15 min of the 2DG treatment, more than 20% cells contained
232 Hsp104-GFP foci indicative of protein aggregation (Fig. 5A, B). In contrast to ATP, the
233 concentration of which recovers to normal levels within 1 min of glucose refeeding (Takaine
234 et al., 2019), the dissolution kinetics of Hsp104-GFP were significantly slower (up to hours,
235 Fig. 5A, B).
236 To further confirm whether a high concentration of ATP is required for protein solubility,
237 we also tested the Ubc9-ts protein, a model protein that is prone to aggregate (Kaganovich,
238 Kopito et al., 2008), and found that ATP depletion by the 2DG treatment triggered Ubc9-ts
239 protein aggregation (Fig. 5C). Thus, not only Hsp104-GFP-positive intrinsic proteins, but also
240 extrinsic model proteins aggregate after ATP depletion.
241

242 SG are assembled in budding yeast cells after stressful conditions, such as glucose depletion
243 (Hoyle et al., 2007). In contrast to the formation of Hsp104-GFP foci, ATP depletion after the
244 2DG treatment did not instantly trigger the formation of SG (Fig. S6). Consistent with recent
245 findings (Jain, Wheeler et al., 2016), the present results suggest that SG formation requires
246 ATP. We also noted that Hsp104-GFP foci and SG did not co-localize, suggesting that these
247 structures are derived from distinct mechanisms (Fig. S6). Thus, the artificial depletion of
248 ATP may trigger abnormal protein aggregation in living yeast cells.
249

250 ATP homeostasis is required for the protection of cells from cytotoxicity caused by
251 protein aggregation
252 Protein aggregation is often associated with neurodegenerative diseases, such as Alzheimer's,
253 Huntington's, and Parkinson's diseases (Eftekharzadeh, Hyman et al., 2016). Mitochondrial
254 failure has also been associated with many neurodegenerative diseases; however, it currently
255 remains unclear whether energy failure causes protein aggregation because mitochondria also
256 produce cytotoxic reactive oxygen species (ROS). (Bhat, Dar et al., 2015, Pathak, Berthet et
257 al., 2013). The abnormal aggregation of α-synuclein has been implicated in Parkinson's
258 disease (Lashuel, Overk et al., 2013). To clarify whether ATP is preventing the formation of
259 cytotoxic protein aggregation, we examined the toxicity of α-synuclein-GFP (Syn-GFP) in
260 budding yeast. As reported previously, the expression of Syn-GFP exhibited negligible
261 toxicity against wild-type yeast when expressed under the inducible *GAL1* promotor (Fig. 6A)
262 (Outeiro & Lindquist, 2003, Sharma, Brandis et al., 2006, Wijayanti, Watanabe et al., 2015).
263 However, *snf1Δ*, *adk1Δ*, and *bas1Δ* are hypersensitive to the expression of Syn-GFP (Fig. 6A).
264 We also found that *rpn4Δ*, which encodes a key transcription factor for proteasomal subunits
265 (Xie & Varshavsky, 2001), was very sensitive to Syn-GFP (Fig. 6A), which is consistent with
266 the concept that Syn-GFP is degraded in the ubiquitin-proteasomal pathway in yeast (Tofaris,
267 Kim et al., 2011, Wijayanti et al., 2015). We then visualized the cellular localization of
268 Syn-GFP. Consistent with previous findings (Willingham, Outeiro et al., 2003), Syn-GFP
269 expressed in yeast mainly localized to the plasma membrane (Fig. 6B, C). In addition to the
270 plasma membrane, we found that Syn-GFP localized to punctated structures, most likely
271 corresponding to protein aggregation (Fig. 6B, C). Punctated structures were not as obvious in
272 *rpn4Δ* cells defective in proteasomes, suggesting that the accumulation of Syn-GFP puncta
273 was not simply due to defective degradation.
274
275 To investigate whether a high concentration of ATP protects cells from toxic protein
276 aggregation, we added extra adenine to the medium (Fig. 6D). A previous study demonstrated
277 that the addition of 300 μM adenine to the medium increased ATP concentrations from 4 to
278 5.5 mM in wild-type cells and from 1 to 4 mM in *bas1Δ* cells (Gauthier et al., 2008) (similar
279 results are shown in Fig. 2D), but induced little or no changes in *adk1Δ* cells (from 2 to 2
280 mM) (Gauthier et al., 2008). Consistent with our hypothesis, the addition of adenine reduced
281 Syn-GFP toxicity and aggregation in *bas1Δ,* but not *adk1Δ* cells (Fig. 6D). Thus, a high
282 concentration of ATP prevented Syn-GFP aggregation and toxicity.
283
284 We examined another model protein involved in neurodegenerative diseases. PolyQ

285 containing the huntingtin protein tends to aggregate and has been implicated in Huntington's
286 disease (Jiang, Poirier et al., 2005). We investigated the toxicity of Htt103Q, a mutant form of
287 the huntingtin protein, which tends to aggregate and cause cytotoxicity in yeast (Meriin,
288 Zhang et al., 2002). Consistent with the concept that a high concentration of ATP prevents
289 protein aggregation, the ATP homeostasis mutants *snf1Δ*, *adk1Δ*, *snf1Δ adk1Δ*, and *bas1Δ*
290 were very sensitive to Htt103Q expression (Fig. S7).
291

292 ## Proteasomes are essential for the removal of protein aggregates caused by ATP
293 depletion

294 Protein aggregation caused by ATP depletion was cytotoxic (Figs. 4B and 6A) and was not
295 easily dissolved after ATP repletion (Fig. 5). To identify a pathway that is essential for the
296 removal of aggregates, we examined the involvement of proteasomes and autophagy.
297
298 The deletion of *RPN4*, which encodes a transcription factor of proteasomal genes (Xie &
299 Varshavsky, 2001), down-regulated proteasomal activity (Kruegel, Robison et al., 2011) and
300 resulted in synthetic growth defects with *adk1Δ*, *snf1Δ bas1Δ* at a high temperature of 38°C
301 and in the presence of H_2O_2 (Fig. 6E). In contrast to proteasomes, autophagy did not appear to
302 have genetic interactions with the above mutants (Fig. 6E). The deletion of an essential
303 component of the autophagic pathway, *ATG1* did not affect the sensitivity of *adk1Δ*, *snf1Δ*,
304 *bas1Δ* to a high temperature of 38°C or to H_2O_2 (Fig. 6E). We also did not observe the
305 accumulation of Hsp104-GFP foci in the autophagy mutants *atg1*, *atg8*, and *atg13* (not
306 shown).
307
308 To investigate the involvement of proteasomes in the removal of protein aggregates after the
309 transient depletion of ATP, we pretreated cells with the proteasomal inhibitor MG132 or
310 DMSO and examined the kinetics for the formation of Hsp104-GFP foci after the 2DG
311 treatment (Fig. 6F) using the drug-sensitive yeast strain Y13206 (Piotrowski, Li et al., 2017).
312 Under both conditions, more than 90% of cells exhibited Hsp104-GFP foci within 30 min of
313 the 2DG treatment. More than two-thirds of Hsp104-GFP foci dissolved in the DMSO control,
314 while less than one-third dissolved in MG132-treated samples, indicating that proteasomes
315 are required for the dissolution process (Fig. 6F).

316 **DISCUSSION**

317 In the present study, we demonstrated for the first time that the Snf1 complex, budding yeast
318 AMPK, is required for the stable maintenance of cellular ATP concentrations (ATP
319 homeostasis) in collaboration with the adenylate kinase Adk1 (Fig. 7A). This function of the
320 Snf1 complex in ATP homeostasis is independent of glucose concentrations in the medium
321 and Mig1, the major transcriptional repressor involved in glucose repression (Fig. 1);
322 therefore, this is distinct from its well-characterized role in adaptation to glucose limitations.
323 The activity of the Snf1 kinase complex may be sharply tuned depending on the intracellular
324 concentrations of adenine nucleotides or other metabolites indicative of cellular energy to
325 prevent a rapid ATP catastrophe (Fig. 3), even in the presence of sufficient amounts of
326 glucose. It is important to note that the reductions observed in intracellular ATP
327 concentrations in *snf1Δ* cells in the presence of glucose were overlooked in previous
328 biochemical analyses, again demonstrating the usefulness of QUEEN-based ATP imaging.
329
330 Since the deletion of *BAS1* caused the greatest reduction in ATP levels and is epistatic to
331 *snf1Δ*, a large pool size of adenine nucleotide is a prerequisite for ATP homeostasis. This
332 assumption is reasonable because the pool size of recyclable ATP restricts ATP
333 concentrations based on the rapid turnover rate of ATP. Bas1 maintains the pool size of ATP
334 by balancing ATP synthesis and irreversible decreases, such as incorporation into RNA and
335 DNA (following conversion to deoxy-ATP), degradation, and excretion in rapidly
336 proliferating yeasts.
337
338 We also showed that key regulators of ATP homeostasis play roles in preventing cytotoxic
339 protein aggregation in budding yeast (Fig. 7B). The common feature associated with these
340 mutants is reduced ATP levels, suggesting that high ATP levels are essential for protein
341 solubilization.
342
343 A recent study suggested that the requirement for ATP changes depending on its
344 concentration. At concentrations lower than 0.5 mM, ATP mainly serves as a substrate for
345 enzymes, such as protein kinases and heat shock protein chaperones, whereas at
346 concentrations higher than 2 mM, ATP may exert solubilizing effects on disordered proteins
347 (Sridharan et al., 2019). ATP homeostasis may also be required to constantly drive
348 proteasomal protein degradation, which requires large amounts of ATP (Benaroudj, Zwickl et
349 al., 2003, Tanaka, Waxman et al., 1983).
350

351 Previous biochemical measurements indicated that although ATP levels were lower in *adk1*
352 and *bas1* mutants than in the wild type, these mutants still had ATP concentrations that were
353 higher than 2 mM (Gauthier et al., 2008), which does not directly explain the accumulation of
354 protein aggregates in these mutants (Fig. 4) because most proteins are expected to be soluble
355 at > 2 mM ATP (Sridharan et al., 2019). The visualization of ATP dynamics in living cells at
356 the single cell level revealed that ATP undergoes transient depletion repeatedly (the ATP
357 catastrophe) in AMPK and ADK mutants, which explains how aggregation-prone proteins
358 aggregate and cause cytotoxicity. A similar, but distinct instability of ATP was observed in
359 *bas1Δ*, further confirming that the ATP catastrophe causes protein aggregation. Although
360 severe ATP depletion in these mutants was gradually recovered by as yet uncharacterized
361 negative feedback regulation, the duration period of ~15 min with reduced ATP levels may
362 induce some proteins to form aggregates that last for generations.
363
364 Many neurodegenerative diseases, such as Alzheimer's, Huntington's, and Parkinson's
365 diseases, are associated with protein aggregation (Eisele, Monteiro et al., 2015, Josefson et al.,
366 2017). On the other hand, mitochondrial dysfunction and accompanying energy failure in
367 nerve cells may result in many types of neurodegenerative diseases based on a large body of
368 evidence (Pathak et al., 2013). For example, previous studies demonstrated that ATP levels in
369 the brain were decreased in patients with early Parkinson's disease (Mochel, N'Guyen et al.,
370 2012) and also that ATP synthesis in the brain was not properly regulated in patients with
371 early Huntington's disease (Hattingen, Magerkurth et al., 2009) and in the corresponding
372 mouse model (Mochel, Durant et al., 2012). Therefore, protein aggregation induced by the
373 ATP catastrophe, as revealed in the present study, may link energy failure and protein
374 aggregation, providing a comprehensive insight into the onset of neurodegenerative diseases.
375 Further studies are warranted to clarify whether the ATP catastrophe also occurs in the
376 neurons of patients at risk of neurodegenerative diseases or in the elderly. However, neither
377 biochemical measurements nor mass spectrometry is capable of detecting the ATP
378 catastrophe because of their insufficient time and space resolution. Thus, an ATP imaging
379 approach using the yeast model system will be the first choice for elucidating the molecular
380 mechanisms underlying ATP homeostasis and ATP catastrophe-induced protein aggregation.
381
382 A recent study reported that the activation of AMPK by metformin ameliorated the
383 progression of Huntington's disease in a mouse model (Arnoux, Willam et al., 2018), and the
384 potential therapeutic use of metformin for neurodegenerative diseases is being discussed
385 (Rotermund, Machetanz et al., 2018). Furthermore, the involvement of ATP and ADKs in

386 preventing the manifestation of Parkinson's disease in mouse models and patients has been
387 proposed (Garcia-Esparcia, Hernandez-Ortega et al., 2015, Nakano, Imamura et al., 2017).
388 Protein aggregation induced by the ATP catastrophe may be a general mechanism for the
389 development of proteinopathies. The present study study using ATP imaging revealed a
390 physiological consequence of a failure in ATP homeostasis in living cells for the first time
391 and suggests that ATP homeostasis has potential as a target for preventing/treating
392 neurodegenerative diseases.

393 **MATERIALS AND METHODS**

394 Yeast strains and plasmids

395 The budding yeast strains and plasmids used in the present study are listed in Supplementary
396 Tables S1 and S2, respectively. These strains were constructed by a PCR-based method
397 (Janke, Magiera et al., 2004) and genetic crosses. The yeast knockout strain collection was
398 originally purchased from GE Healthcare (cat. # YSC1053).
399

400 Media and cell culture

401 The standard technique for the yeast culture and manipulation was used (Guthrie & Fink,
402 2002). Synthetic medium (SC) was prepared according to the recipe of Hanscho et al.
403 (Hanscho, Ruckerbauer et al., 2012). 2-Deoxy-D-glucose (2DG), tunicamycin, and MG132
404 were purchased from FUJIFILM Wako (cat. # 046-06483, 202-08241, and 139-18451,
405 respectively). Tunicamycin and MG132 were dissolved in dimethylsulfoxide (DMSO) to
406 make stock solutions (5 mg/ml and 42 mM, respectively). Cells were grown to the mid-log
407 phase at 30°C in SC before imaging unless otherwise noted.
408

409 Microscopy

410 Cells expressing Hsp104-GFP or GFP-Ubc9ts were concentrated by centrifugation and
411 sandwiched between a slide and coverslip (No. 1.5 thickness, Matsunami, Osaka, Japan).
412 Immobilized cells were imaged using an inverted fluorescent microscope (Eclipse Ti-E,
413 Nikon) equipped with an Apo TIRF 100× Oil DIC N2/NA 1.49 objective lens and
414 electron-multiplying charge-coupled device camera (iXon3 DU897E-CS0-#BV80, Andor) at
415 approximately 25°C. The Hsp104-GFP and GFP-Ubc9ts fluorescent signal was collected
416 from stacks of 11 *z*-sections spaced by 0.5 μm, and the maximum projections of the optical
417 sections were shown in Figs. 4, 5, and S6. Cells expressing QUEEN were immobilized on a
418 concanavalin A-coated 35-mm glass-bottomed dish (#3971-035, No. 1.5 thickness, IWAKI).
419 The dish was filled with an excess amount of medium (4.5–5 ml) against the cell volume to
420 minimize changes in the chemical compositions of the medium during observations. QUEEN
421 fluorescence was acquired as previously described (Takaine et al., 2019). Cells expressing
422 α-synuclein-GFP were immobilized on a slide glass as described above, and the fluorescence
423 signal was collected from a single *z*-plane using an inverted fluorescent microscope (Eclipse
424 Ti2-E, Nikon, Tokyo, Japan) equipped with a CFI Plan Apoλ100× Oil DIC/NA1.45 objective

425 lens and CMOS image sensor (DS-Qi2, Nikon). Images of cells were acquired from several
426 fields of view for each experimental condition.
427

428 ## Data analysis

429 Numerical data were plotted using KaleidaGraph software ver. 4.5.1 (Synergy Software).
430 Means, SDs, and *p* values were calculated using Excel software (Microsoft, WA, US).
431 Significance between two sets of data was tested using the unpaired one-tailed Welch's *t*-test
432 unless otherwise noted, and was indicated by an asterisk or *p* value. The horizontal bar in the
433 dot plot indicates the average of each population. All measurements were repeated at least
434 twice to confirm reproducibility.
435 ATP concentrations in yeast cells were estimated using QUEEN-based ratiometric
436 imaging, as previously described (Takaine, 2019, Takaine et al., 2019). The QUEEN ratio is
437 proportional to ATP concentrations and pseudo-colored to reflect its value throughout the
438 present study. The mean QUEEN ratio inside of a cell represents the intracellular ATP
439 concentration of the cell.
440 The autocorrelation functions (ACF) of oscillations in the QUEEN ratio were
441 calculated using R studio software ver. 3.4.1 (R Core Team, 2017). The apparent period of
442 oscillation was estimated from the positive second peak of the correlation coefficient, which
443 was outside the 95% confidence interval and significant ($p < 0.05$), rejecting the assumption
444 that there is no correlation.
445

ACKNOWLEDGMENTS

We are grateful to the Yeast Genetic Resource Center, Y. Ohya, K. Ohashi, H. Takagi, D. Watanabe, and J. Frydman for providing the yeast strains and plasmids. We thank the members of the Yoshida/Takaine labs for their support. This work was supported by JSPS grants 16H04781 (S.Y. and M.T.) and 15K18525 (M.T.) and the Takeda Science foundation (S.Y.). This work was also supported by the joint research program of the Institute for Molecular and Cellular Regulation, Gunma University, Japan.

AUTHOR CONTRIBUTIONS

M.T. and S.Y. conceived and designed the project. M.T. conducted experiments and the data analysis. H.I. provided a key reagent and expertise. M.T. and S.Y wrote the manuscript with input from H.I.

CONFLICT OF INTEREST

The authors declare no competing interests.

461 **REFERENCES**

462 Arnoux I, Willam M, Griesche N, Krummeich J, Watari H, Offermann N, Weber S, Narayan Dey P, Chen C,
463 Monteiro O, Buettner S, Meyer K, Bano D, Radyushkin K, Langston R, Lambert JJ, Wanker E, Methner A,
464 Krauss S, Schweiger S et al. (2018) Metformin reverses early cortical network dysfunction and behavior changes
465 in Huntington's disease. *Elife* 7

466 Baryshnikova A (2016) Systematic Functional Annotation and Visualization of Biological Networks. *Cell*
467 *Syst* 2: 412-21

468 Benaroudj N, Zwickl P, Seemuller E, Baumeister W, Goldberg AL (2003) ATP hydrolysis by the proteasome
469 regulatory complex PAN serves multiple functions in protein degradation. *Mol Cell* 11: 69-78

470 Bhat AH, Dar KB, Anees S, Zargar MA, Masood A, Sofi MA, Ganie SA (2015) Oxidative stress,
471 mitochondrial dysfunction and neurodegenerative diseases; a mechanistic insight. *Biomed Pharmacother* 74:
472 101-10

473 Carlson M (1999) Glucose repression in yeast. *Curr Opin Microbiol* 2: 202-7

474 Cherry JM, Hong EL, Amundsen C, Balakrishnan R, Binkley G, Chan ET, Christie KR, Costanzo MC,
475 Dwight SS, Engel SR, Fisk DG, Hirschman JE, Hitz BC, Karra K, Krieger CJ, Miyasato SR, Nash RS, Park J,
476 Skrzypek MS, Simison M et al. (2012) Saccharomyces Genome Database: the genomics resource of budding
477 yeast. *Nucleic Acids Res* 40: D700-5

478 Daignan-Fornier B, Fink GR (1992) Coregulation of purine and histidine biosynthesis by the transcriptional
479 activators BAS1 and BAS2. *Proc Natl Acad Sci U S A* 89: 6746-50

480 Denis V, Boucherie H, Monribot C, Daignan-Fornier B (1998) Role of the myb-like protein bas1p in
481 Saccharomyces cerevisiae: a proteome analysis. *Mol Microbiol* 30: 557-66

482 Edelman AM, Blumenthal DK, Krebs EG (1987) Protein serine/threonine kinases. *Annu Rev Biochem* 56:
483 567-613

484 Eftekharzadeh B, Hyman BT, Wegmann S (2016) Structural studies on the mechanism of protein aggregation
485 in age related neurodegenerative diseases. *Mech Ageing Dev* 156: 1-13

486 Eisele YS, Monteiro C, Fearns C, Encalada SE, Wiseman RL, Powers ET, Kelly JW (2015) Targeting
487 protein aggregation for the treatment of degenerative diseases. *Nat Rev Drug Discov* 14: 759-80

488 Garcia-Esparcia P, Hernandez-Ortega K, Ansoleaga B, Carmona M, Ferrer I (2015) Purine metabolism gene
489 deregulation in Parkinson's disease. *Neuropathol Appl Neurobiol* 41: 926-40

490 Gauthier S, Coulpier F, Jourdren L, Merle M, Beck S, Konrad M, Daignan-Fornier B, Pinson B (2008)
491 Co-regulation of yeast purine and phosphate pathways in response to adenylic nucleotide variations. *Mol*
492 *Microbiol* 68: 1583-94

493 Ghillebert R, Swinnen E, Wen J, Vandesteene L, Ramon M, Norga K, Rolland F, Winderickx J (2011) The
494 AMPK/SNF1/SnRK1 fuel gauge and energy regulator: structure, function and regulation. *FEBS J* 278: 3978-90

495 Guthrie C, Fink GR (2002) *Guide to yeast genetics and molecular and cell Biology: Part C*. Gulf Professional

496 Publishing,
497 Hanscho M, Ruckerbauer DE, Chauhan N, Hofbauer HF, Krahulec S, Nidetzky B, Kohlwein SD, Zanghellini
498 J, Natter K (2012) Nutritional requirements of the BY series of Saccharomyces cerevisiae strains for optimum
499 growth. *FEMS Yeast Res* 12: 796-808
500 Hardie DG, Carling D, Carlson M (1998) The AMP-activated/SNF1 protein kinase subfamily: metabolic
501 sensors of the eukaryotic cell? *Annu Rev Biochem* 67: 821-55
502 Hardie DG, Schaffer BE, Brunet A (2016) AMPK: An Energy-Sensing Pathway with Multiple Inputs and
503 Outputs. *Trends Cell Biol* 26: 190-201
504 Hattingen E, Magerkurth J, Pilatus U, Mozer A, Seifried C, Steinmetz H, Zanella F, Hilker R (2009)
505 Phosphorus and proton magnetic resonance spectroscopy demonstrates mitochondrial dysfunction in early and
506 advanced Parkinson's disease. *Brain* 132: 3285-97
507 Hayes MH, Peuchen EH, Dovichi NJ, Weeks DL (2018) Dual roles for ATP in the regulation of phase
508 separated protein aggregates in Xenopus oocyte nucleoli. *eLife* 7: e35224
509 Hedbacker K, Carlson M (2008) SNF1/AMPK pathways in yeast. *Front Biosci* 13: 2408-20
510 Herzig S, Shaw RJ (2017) AMPK: guardian of metabolism and mitochondrial homeostasis. *Nat Rev Mol Cell*
511 *Biol* 19: 121
512 Hoyle NP, Castelli LM, Campbell SG, Holmes LE, Ashe MP (2007) Stress-dependent relocalization of
513 translationally primed mRNPs to cytoplasmic granules that are kinetically and spatially distinct from P-bodies. *J*
514 *Cell Biol* 179: 65-74
515 Jain S, Wheeler JR, Walters RW, Agrawal A, Barsic A, Parker R (2016) ATPase-Modulated Stress Granules
516 Contain a Diverse Proteome and Substructure. *Cell* 164: 487-98
517 Janke C, Magiera MM, Rathfelder N, Taxis C, Reber S, Maekawa H, Moreno-Borchart A, Doenges G,
518 Schwob E, Schiebel E, Knop M (2004) A versatile toolbox for PCR-based tagging of yeast genes: new
519 fluorescent proteins, more markers and promoter substitution cassettes. *Yeast* 21: 947-62
520 Janssen E, Dzeja PP, Oerlemans F, Simonetti AW, Heerschap A, de Haan A, Rush PS, Terjung RR, Wieringa
521 B, Terzic A (2000) Adenylate kinase 1 gene deletion disrupts muscle energetic economy despite metabolic
522 rearrangement. *EMBO J* 19: 6371-81
523 Jiang H, Poirier MA, Ross CA (2005) A structure-based analysis of huntingtin mutant polyglutamine
524 aggregation and toxicity: evidence for a compact beta-sheet structure. *Hum Mol Genet* 14: 765-774
525 Josefson R, Andersson R, Nyström T (2017) How and why do toxic conformers of aberrant proteins
526 accumulate during ageing? *Essays Biochem* 61: 317
527 Kaganovich D, Kopito R, Frydman J (2008) Misfolded proteins partition between two distinct quality control
528 compartments. *Nature* 454: 1088-95
529 Kruegel U, Robison B, Dange T, Kahlert G, Delaney JR, Kotireddy S, Tsuchiya M, Tsuchiyama S,
530 Murakami CJ, Schleit J, Sutphin G, Carr D, Tar K, Dittmar G, Kaeberlein M, Kennedy BK, Schmidt M (2011)

531 Elevated proteasome capacity extends replicative lifespan in Saccharomyces cerevisiae. *PLoS Genet* 7:
532 e1002253
533 Lashuel HA, Overk CR, Oueslati A, Masliah E (2013) The many faces of alpha-synuclein: from structure and
534 toxicity to therapeutic target. *Nat Rev Neurosci* 14: 38-48
535 Ljungdahl PO, Daignan-Fornier B (2012) Regulation of amino acid, nucleotide, and phosphate metabolism in
536 Saccharomyces cerevisiae. *Genetics* 190: 885-929
537 Meriin AB, Zhang X, He X, Newnam GP, Chernoff YO, Sherman MY (2002) Huntington toxicity in yeast
538 model depends on polyglutamine aggregation mediated by a prion-like protein Rnq1. *J Cell Biol* 157: 997-1004
539 Mochel F, Durant B, Meng X, O'Callaghan J, Yu H, Brouillet E, Wheeler VC, Humbert S, Schiffmann R,
540 Durr A (2012) Early alterations of brain cellular energy homeostasis in Huntington disease models. *J Biol Chem*
541 287: 1361-70
542 Mochel F, N'Guyen TM, Deelchand D, Rinaldi D, Valabregue R, Wary C, Carlier PG, Durr A, Henry PG
543 (2012) Abnormal response to cortical activation in early stages of Huntington disease. *Mov Disord* 27: 907-10
544 Mortensen SP, Thaning P, Nyberg M, Saltin B, Hellsten Y (2011) Local release of ATP into the arterial
545 inflow and venous drainage of human skeletal muscle: insight from ATP determination with the intravascular
546 microdialysis technique. *The Journal of Physiology* 589: 1847-1857
547 Nakano M, Imamura H, Sasaoka N, Yamamoto M, Uemura N, Shudo T, Fuchigami T, Takahashi R,
548 Kakizuka A (2017) ATP Maintenance via Two Types of ATP Regulators Mitigates Pathological Phenotypes in
549 Mouse Models of Parkinson's Disease. *EBioMedicine* 22: 225-241
550 Outeiro TF, Lindquist S (2003) Yeast cells provide insight into alpha-synuclein biology and pathobiology.
551 *Science* 302: 1772-5
552 Patel A, Malinovska L, Saha S, Wang J, Alberti S, Krishnan Y, Hyman AA (2017) ATP as a biological
553 hydrotrope. *Science* 356: 753-756
554 Pathak D, Berthet A, Nakamura K (2013) Energy failure: does it contribute to neurodegeneration? *Ann*
555 *Neurol* 74: 506-16
556 Piotrowski JS, Li SC, Deshpande R, Simpkins SW, Nelson J, Yashiroda Y, Barber JM, Safizadeh H, Wilson
557 E, Okada H, Gebre AA, Kubo K, Torres NP, LeBlanc MA, Andrusiak K, Okamoto R, Yoshimura M,
558 DeRango-Adem E, van Leeuwen J, Shirahige K et al. (2017) Functional annotation of chemical libraries across
559 diverse biological processes. *Nature Chemical Biology* 13: 982
560 R Core Team (2017) R: A Language and Environment for Statistical Computing. In Vienna, Austria: R
561 Foundation for Statistical Computing
562 Rotermund C, Machetanz G, Fitzgerald JC (2018) The Therapeutic Potential of Metformin in
563 Neurodegenerative Diseases. *Front Endocrinol (Lausanne)* 9: 400
564 Sharma N, Brandis KA, Herrera SK, Johnson BE, Vaidya T, Shrestha R, DebBurman SK (2006) α-synuclein
565 budding yeast model. *J Mol Neurosci* 28: 161-178

566 Sridharan S, Kurzawa N, Werner T, Günthner I, Helm D, Huber W, Bantscheff M, Savitski MM (2019)
567 Proteome-wide solubility and thermal stability profiling reveals distinct regulatory roles for ATP. *Nature*
568 *Communications* 10: 1155
569 Takaine M (2019) QUEEN-based Spatiotemporal ATP Imaging in Budding and Fission Yeast. *Bio-protocol*
570 9: e3320
571 Takaine M, Ueno M, Kitamura K, Imamura H, Yoshida S (2019) Reliable imaging of ATP in living budding
572 and fission yeast. *J Cell Sci* 132
573 Tanaka K, Waxman L, Goldberg AL (1983) ATP serves two distinct roles in protein degradation in
574 reticulocytes, one requiring and one independent of ubiquitin. *J Cell Biol* 96: 1580-5
575 Tofaris GK, Kim HT, Hourez R, Jung JW, Kim KP, Goldberg AL (2011) Ubiquitin ligase Nedd4 promotes
576 alpha-synuclein degradation by the endosomal-lysosomal pathway. *Proc Natl Acad Sci U S A* 108: 17004-9
577 Usaj M, Tan Y, Wang W, VanderSluis B, Zou A, Myers CL, Costanzo M, Andrews B, Boone C (2017)
578 TheCellMap.org: A Web-Accessible Database for Visualizing and Mining the Global Yeast Genetic Interaction
579 Network. *G3 (Bethesda)* 7: 1539-1549
580 Wijayanti I, Watanabe D, Oshiro S, Takagi H (2015) Isolation and functional analysis of yeast ubiquitin
581 ligase Rsp5 variants that alleviate the toxicity of human α-synuclein. *The Journal of Biochemistry* 157: 251-260
582 Willingham S, Outeiro TF, DeVit MJ, Lindquist SL, Muchowski PJ (2003) Yeast genes that enhance the
583 toxicity of a mutant huntingtin fragment or alpha-synuclein. *Science* 302: 1769-72
584 Wilson WA, Hawley SA, Hardie DG (1996) Glucose repression/derepression in budding yeast: SNF1 protein
585 kinase is activated by phosphorylation under derepressing conditions, and this correlates with a high AMP:ATP
586 ratio. *Curr Biol* 6: 1426-34
587 Xiao B, Heath R, Saiu P, Leiper FC, Leone P, Jing C, Walker PA, Haire L, Eccleston JF, Davis CT, Martin
588 SR, Carling D, Gamblin SJ (2007) Structural basis for AMP binding to mammalian AMP-activated protein
589 kinase. *Nature* 449: 496-500
590 Xie Y, Varshavsky A (2001) RPN4 is a ligand, substrate, and transcriptional regulator of the 26S
591 proteasome: a negative feedback circuit. *Proc Natl Acad Sci U S A* 98: 3056-61
592 Yaginuma H, Kawai S, Tabata KV, Tomiyama K, Kakizuka A, Komatsuzaki T, Noji H, Imamura H (2014)
593 Diversity in ATP concentrations in a single bacterial cell population revealed by quantitative single-cell imaging.
594 *Sci Rep* 4: 6522
595

596 **FIGURE LEGENDS**

597 Fig. 1 AMPK is involved in the maintenance of cellular ATP levels in non-starving cells

598 (A) Visualization of intracellular ATP levels in wild-type (WT) and *snf1Δ* cells using the
599 ATP sensor QUEEN. Cells were grown to the mid-log phase in SC-H medium containing the
600 indicated concentrations of glucose and then imaged. White scale bar = 5 μm. (B) *snf1Δ* cells
601 had lower ATP levels than wild-type cells. The mean QUEEN ratio inside a single cell (mean
602 QUEEN ratio/cell), which represents the intracellular ATP level of the cell, was quantified for
603 each cell from the ratio image. Data are the mean of the cell population ± 1SD (error bar)
604 normalized to wild-type cells. N = 105–193 cells were scored. Asterisks indicate a significant
605 difference from WT ($p < 0.05$). (C) ATP levels in single-deletion mutants of AMPK *β*
606 subunits. Data are the mean of the cell population ± 1SD (error bar) normalized to wild-type
607 cells. N = 177–223 cells were scored. Asterisks indicate a significant difference between the
608 two strains (*, $p < 0.05$; **, $p < 0.01$). N.S., no significance. (D) *mig1Δ* cells had slightly
609 lower ATP levels than wild-type cells. Data are the mean of the cell population ± 1SD (error
610 bar) normalized to wild-type cells. N = 190–231 cells were scored. Asterisks indicate a
611 significant difference between the two strains.

612

613 Fig. 2 Interconversion and active synthesis of adenine nucleotides are important for
614 ATP homeostasis

615 (A) Adk1 and Snf1 synergistically control cellular ATP levels. QUEEN ratio images of ATP
616 homeostasis mutant cells grown in the medium containing 2% glucose. The asterisk indicates
617 an example of cells with significantly reduced ATP levels. (B) Mean QUEEN ratios of cells
618 were translated to ATP concentrations and shown in a dot plot. The horizontal bar indicates
619 the mean of each population. Asterisks indicate *p* values versus WT: *=1.5×10^{-59},
620 **=2.3×10^{-34}, ***=2.9×10^{-117}. CV: coefficient of variance. N = 134–276 cells were scored.
621 (C) QUEEN ratio images of *bas1Δ* cells grown in the 2% glucose medium. Growth in media
622 supplemented with 0.11 mg/ml adenine partially restored the low ATP phenotype of *bas1*Δ.
623 (D) The ATP concentrations of cells shown in (C) were plotted. Asterisks indicate *p* values:
624 *=2.3×10^{-160}, **=8.8×10^{-12} (versus WT in glucose), ***=3.6×10^{-20} (versus *bas1*Δ in glucose).
625 CV: coefficient of variance. N = 186–296 cells were scored.

626

627 Fig. 3 Temporal fluctuations in ATP levels in *snf1*Δ*adk1*Δ and *bas1*Δ cells

628 (A, C) Time-lapse imaging of QUEEN in *snf1*Δ *adk1*Δ cells in the 2% glucose medium.
629 Images at the representative time points were shown. The QUEEN ratio decreased twice
630 (indicated by arrowheads) within a short interval. See also Movie S1. Data were converted

631 into ATP concentrations and plotted in (C). (B, D) Another example of time-lapse imaging of
632 QUEEN in *snf1*Δ*adk1*Δ cells in the 2% glucose medium. The QUEEN ratio decreased twice
633 (indicated by arrowheads) with a long interval. See also Movie S2. Data were converted into
634 ATP concentrations and plotted in (D). (E) Time-lapse imaging of QUEEN in *bas1*Δ in the
635 2% glucose medium. The ATP concentrations of the mother (cell-1) and daughter (cell-2)
636 were plotted at the bottom. Images at the representative time points were shown on the top.
637 Note that the QUEEN ratio is synchronized until cells undergo separation at the time point of
638 76 min indicated by an arrow. After separation, each cell has a unique periodic cycle of ATP.
639 The movie is available in Movie S3. White scale bar = 5 μm.
640
641 Fig. 4 ATP homeostasis is required to prevent protein aggregation
642 (A) Functional landscape of known interactors of ATP mutants. Negative genetic interactors
643 of the indicated gene were derived from the SGD database (https://www.yeastgenome.org/)
644 (Cherry, Hong et al., 2012) and overlaid on a functional map based on the global genetic
645 interaction network of the yeast genome (Baryshnikova, 2016, Usaj et al., 2017). *URA6*
646 encodes an uridylate kinase that is essential for viability, which also exhibits adenylate kinase
647 activity. (B) Each strain of the indicated genotype was serially diluted (five-fold), spotted on
648 the SC + 2% glucose medium, and grown under the indicated stress conditions. Photos were
649 taken after 2-3 days. (C) Formation of Hsp104-GFP foci in ATP homeostasis mutants. The
650 GFP signal (inverted grayscale) was imaged in the log phase culture of the indicated mutant
651 cells expressing Hsp104-GFP at 35°C. (D) Quantification of data shown in (C). Data from
652 similar experiments using strains expressing Pab1-GFP, instead of Hsp104-GFP, were also
653 plotted. Values are the mean ± 1SD (error bars). Asterisks indicate a significant difference
654 from WT ($p < 0.05$) (N=3–4). White scale bar = 5 μm.
655
656 Fig. 5 ATP depletion triggers protein aggregation in living yeast cells
657 (A) The formation of Hsp104-GFP foci after ATP depletion. Wild-type cells expressing
658 Hsp104-GFP were grown to the log phase at 35°C in the medium containing 2% glucose. At
659 the time point of 0 min, the medium was replaced with 20 mM 2DG (red) or 2% glucose (as a
660 control; blue). Cells were released back to media containing 2% glucose at the time point of
661 50 min. Cells were imaged at the indicated time points, classified, and scored according to the
662 number of Hsp104-GFP foci. Values are the mean (N = 3). Asterisks indicate a significant
663 difference from the 2% glucose treatment ($p < 0.05$). (B) Representative images of cells
664 analyzed in (A). (C) Formation of Ubc9-ts foci after ATP depletion. Cells expressing
665 GFP-Ubc9-ts under an inducible *GAL* promoter were grown in the medium containing 2%

666 galactose (SC-gal) at 33°C, and the medium was then exchanged with 2DG or SC-gal. After
667 30 min, cells were imaged and scored for the number of GFP-Ubc9-ts foci. Representative
668 images (inverted grayscale) are shown on the left and summarized on the right. Values are the
669 mean ± 1SD (error bars) (N = 4). White scale bar = 5 μm.
670
671 Fig. 6 Aggregation and cytotoxicity of α-synuclein depends on ATP homeostasis
672 (A) Each strain of the indicated genotype was transformed with an expression vector carrying
673 α-synuclein-GFP or GFP, serially diluted (five-fold), spotted on SC + 2% galactose plates,
674 and then grown at 30°C for 3 days. (B) The localization of α-synuclein-GFP in ATP mutants.
675 Cells were grown on galactose plates at 30°C for more than 42 h and then imaged.
676 Representative images of α-synuclein-GFP (inverted grayscale) are shown. (C) Quantification
677 of the data shown in (B). Cells were classified and scored for the localization pattern of
678 α-synuclein-GFP. The percentage of cells showing α-synuclein-GFP foci are plotted. Data are
679 the mean ± 1SD (error bars) from 3–6 independent observations. N = 33–380 cells were
680 scored in each measurement. *P* values versus WT are shown. N.S., no significance (p value >
681 0.05). (D) *(top)* Each strain of the indicated genotype was transformed with an expression
682 vector carrying α-synuclein-GFP and grown on galactose plates containing 0 mM (−
683 Adenine) or 0.3 mM (+ Adenine) adenine at 30°C for 3 days. *(bottom)* Cells were grown on
684 galactose plates in the absence or presence of adenine at 30°C for 41-45 h and then imaged.
685 The percentage of cells showing α-synuclein-GFP foci were plotted. Data are the mean ± 1SD
686 (error bars) from 5 independent transformants. N = 53–258 cells were scored in each
687 measurement. *P* values versus "– Adenine" are shown. (E) Each strain of the indicated
688 genotype was serially diluted (five-fold), spotted on the SC + 2% glucose medium, and grown
689 under the indicated stress conditions. (F) Cells of the drug-sensitive strain Y13206 were
690 grown to the log phase at 37°C in the medium containing 2% glucose and supplemented with
691 0.1% DMSO or 0.1% DMSO plus 42 μM MG132 at $t = -30$ min. At $t = 0$ min, these cells
692 were washed and released in the medium containing 20 mM 2DG ± MG132, and the cells
693 were then washed and released again in the medium containing 2% glucose ± MG132. Cells
694 were imaged at the indicated time points and scored for the number of Hsp104-GFP foci.
695 Data are the mean ± 1SD (error bars). Asterisks indicate a significant difference from DMSO
696 ($p < 0.02$) (N=3).
697
698 Fig. 7 Models for ATP homeostasis and its role in proteostasis
699 (A) Schematic summary of the roles of Snf1, Adk1, and Bas1 in ATP homeostasis. (B) A
700 schematic model for ATP homeostasis preventing cytotoxic protein aggregation.

701 **SUPPLEMENTARY INFORMATION**

702 Supplementary figure legends

703 Fig. S1 Adenylate kinase Adk1 is involved in the maintenance of cellular ATP
704 concentrations

705 (A) QUEEN ratio images of wild-type and *adk1Δ* cells grown in 2% glucose or 2% galactose.
706 White scale bar = 5 μm. (B) Quantification of data shown in (A). The mean QUEEN ratio/cell
707 was quantified for each cell from ratio images. Values are the mean of the cell population ±
708 1SD (error bar). N = 182–236 cells were scored. Asterisks indicate a significant difference
709 from WT ($p < 0.05$).

710

711 Fig. S2 ATP levels in *bas1*Δ *snf1*Δ cells

712 (A) QUEEN ratio images of wild-type, *bas1Δ*, *snf1Δ*, and *bas1Δ snf1Δ* cells. (B)
713 Quantification of data shown in (A). The mean QUEEN ratio/cell was quantified for each cell
714 from ratio images. Data are shown as a dot plot. The horizontal bar in the plot indicates the
715 mean of each population. Significance between two sets of data was tested using the unpaired
716 two-tailed Welch's *t*-test and indicated by *p* values. N.S., no significance (*p*-value > 0.05).

717

718 Fig. S3 Time-lapse imaging of QUEEN in *snf1*Δ *adk1*Δ cells

719 Time-lapse imaging of QUEEN in *snf1*Δ *adk1*Δ cells in the 2% glucose medium. An example
720 of *snf1*Δ *adk1*Δ cell showing an irreversible decrease in the QUEEN ratio (indicated by an
721 arrowhead). In this case, the cell eventually died (indicated by an arrow). Images at the
722 representative time points were shown. The ATP concentration was plotted at the bottom.
723 White scale bar = 5 μm.

724

725 Fig. S4. Oscillatory behavior of the ATP concentration visualized in *bas1*Δ cells

726 (A) Another example of *bas1Δ* cells showing an oscillating QUEEN ratio. In this case,
727 cytokinesis had just been completed at t = 0 min. ATP concentrations in cell-1 and cell-2 were
728 plotted at the bottom. See also Movie S4. White scale bar = 5 μm. (B) Autocorrelation
729 function of the QUEEN ratio calculated from the data on cell-1 in Fig. 3E. Blue dotted lines
730 indicate the 95% confidence interval. An arrow indicates the second peak of the correlation
731 and corresponds to the apparent period.

732

733 Fig. S5 *In silico* analysis of interactors of ATP mutants

734 Genetic and physical interactors of the indicated genes were derived from the SGD database
735 (https://www.yeastgenome.org/) (Cherry et al., 2012) and overlaid on a functional map based

736 on the global genetic interaction network of the yeast genome (Baryshnikova, 2016, Usaj et
737 al., 2017). *URA6* encodes an uridylate kinase essential for viability, which also exhibits
738 adenylate kinase activity.
739
740 Fig. S6 Simultaneous observation of Hsp104 and Pab1 foci
741 Wild-type cells expressing Hsp104-GFP and Pab1-RedStar2 were grown to the log phase at
742 37°C in the medium containing 2% glucose. Cells were washed and released either in the
743 medium containing 20 mM 2DG (top) or in the medium lacking glucose (bottom), and then
744 imaged after 30 and 60 min. White scale bar = 5 μm.
745
746 Fig. S7 Cytotoxicity of polyQ containing the huntingtin protein in wild-type and
747 ATP-mutant yeast cells
748 Each strain of the indicated genotype was transformed with an expression vector carrying
749 Htt103Q and grown on glucose ((-), no induction) or raffinose ((+), leaky expression) plates
750 at 30°C for 3 days.
751

752 Table S1. *Strains used in the present study*

Name	Genotype	Source	Figure
MTY3008	*snf1Δ::kanMX6 leu2Δ0 lys2Δ0 ura3Δ0*	Lab stock	4B, 6A-C, 6E, S7
MTY3015	*his3Δ1 leu2Δ0 lys2Δ0 ura3Δ0*	Lab stock	4B, 6A-E, S7
MTY3049	*adk1Δ::kanMX6 his3Δ1 leu2Δ0 lys2Δ0 ura3Δ0*	Lab stock	4B, 6A-E, S7
MTY3118	*bas1Δ::kanMX6 leu2Δ0 lys2Δ0 ura3Δ0*	Lab stock	4B, 6A-E, S7
MTY3143	*his3Δ1:: 2×pRS303-P_{TEF}-QUEEN-2m-T_{CYC1} leu2Δ0 lys2Δ0 ura3Δ0*	This study	S1
MTY3149	*adk1Δ::kanMX6 his3Δ1:: 2×pRS303-P_{TEF}-QUEEN-2m-T_{CYC1} leu2Δ0 lys2Δ0 ura3Δ0*	This study	S1
MTY3264	*his3Δ1:: 3×pRS303-P_{TEF}-QUEEN-2m-T_{CYC1} leu2Δ0 lys2Δ0 ura3Δ0 MYO1-3mCherry-hphMX6*	Takaine et al., 2019	2A, B, S2
MTY3270	*bas1Δ::kanMX6 his3Δ1:: 3×pRS303-P_{TEF}-QUEEN-2m-T_{CYC1} leu2Δ0 lys2Δ0 ura3Δ0 MYO1-3mCherry-hphMX6*	This study	2C, D, 3E, S2, S4
MTY3293	*adk1Δ::kanMX6 his3Δ1:: 3×pRS303-P_{TEF}-QUEEN-2m-T_{CYC1} leu2Δ0 lys2Δ0 ura3Δ0 MYO1-3mCherry-hphMX6*	This study	2A, B
MTY3355	*adk1Δ::kanMX6 snf1Δ::natNT2 his3Δ1:: 3×pRS303-P_{TEF}-QUEEN-2m-T_{CYC1} leu2Δ0 lys2Δ0 ura3Δ0 MYO1-3mCherry-hphMX6*	This study	2A, B, 3A-D, S3
MTY3371	*snf1Δ::kanMX6 his3Δ1:: 3×pRS303-P_{TEF}-QUEEN-2m-T_{CYC1} leu2Δ0 lys2Δ0 ura3Δ0 MYO1-3mCherry-hphMX6*	This study	2A, B, S2
MTY3412	*adk1Δ::kanMX6 snf1Δ::natNT2 leu2Δ0 lys2Δ0 ura3Δ0*	This study	4B, 6A-E, S7
MTY3420	*Hsp104-yeGFP-hphNT1 his3Δ1 leu2Δ0 lys2Δ0 ura3Δ0*	This study	4C, D, 5A, B
MTY3421	*snf1Δ::kanMX6 Hsp104-yeGFP-hphNT1 his3Δ1 leu2Δ0 lys2Δ0 ura3Δ0*	This study	4C, D
MTY3422	*bas1Δ::kanMX6 Hsp104-yeGFP-hphNT1 his3Δ1 leu2Δ0 lys2Δ0 ura3Δ0*	This study	4C, D
MTY3424	*adk1Δ::kanMX6 Hsp104-yeGFP-hphNT1 his3Δ1 leu2Δ0 lys2Δ0 ura3Δ0*	This study	4C-D
MTY3425	*adk1Δ::kanMX6 snf1Δ::natNT2 Hsp104-yeGFP-hphNT1 his3Δ1 leu2Δ0 lys2Δ0 ura3Δ0*	This study	4C, D
MTY3489	*atg1Δ::kanMX6 his3Δ1 leu2Δ0 lys2Δ0 ura3Δ0*	Lab stock	6E
MTY3493	*snq2Δ::KILeu2; pdr3Δ::KIura3; pdr1Δ::natMX4; can1Δ::STE2prSp_his5 lyp1Δ*	From Y.	Parental

	his3Δ1 leu2Δ0 ura3Δ0 met15Δ0 LYS2+	Ohya, (Piotrowski et al., 2017)	strain of MTY3501
MTY3501	*Hsp104-yeGFP-hphNT1 snq2Δ::KILeu2; pdr3Δ::KIura3; pdr1Δ::natMX4; can1Δ::STE2prSp_his5 lyp1Δ his3Δ1 leu2Δ0 ura3Δ0 met15Δ0 LYS2+*	This study	6F
MTY3503	*Pab1- yeGFP-hphNT1 his3Δ1 leu2Δ0 lys2Δ0 ura3Δ0*	This study	4D
MTY3504	*Hsp104-yeGFP-hphNT1 Pab1-RedStar2-natNT2 his3Δ1 leu2Δ0 lys2Δ0 ura3Δ0*	This study	S6
MTY3505	*snf1Δ::kanMX6 Pab1- yeGFP-hphNT1 his3Δ1 leu2Δ0 lys2Δ0 ura3Δ0*	This study	4D
MTY3506	*adk1Δ::kanMX6 Pab1- yeGFP-hphNT1 his3Δ1 leu2Δ0 lys2Δ0 ura3Δ0*	This study	4D
MTY3507	*adk1Δ::kanMX6 snf1Δ::natNT2 Pab1- yeGFP-hphNT1 his3Δ1 leu2Δ0 lys2Δ0 ura3Δ0*	This study	4D
MTY3508	*bas1Δ::kanMX6 Pab1- yeGFP-hphNT1 his3Δ1 leu2Δ0 lys2Δ0 ura3Δ0*	This study	4D
MTY3513	*atg1Δ::natNT2 adk1Δ::kanMX6 his3Δ1 leu2Δ0 lys2Δ0 ura3Δ0*	This study	6E
MTY3514	*atg1Δ::natNT2 snf1Δ::kanMX6 his3Δ1 leu2Δ0 lys2Δ0 ura3Δ0*	This study	6E
MTY3515	*atg1Δ::natNT2 bas1Δ::kanMX6 his3Δ1 leu2Δ0 lys2Δ0 ura3Δ0*	This study	6E
MTY3516	*rpn4Δ::natNT2 adk1Δ::kanMX6 his3Δ1 leu2Δ0 lys2Δ0 ura3Δ0*	This study	6E
MTY3517	*rpn4Δ::natNT2 snf1Δ::kanMX6 his3Δ1 leu2Δ0 lys2Δ0 ura3Δ0*	This study	6E
MTY3518	*rpn4Δ::natNT2 bas1Δ::kanMX6 his3Δ1 leu2Δ0 lys2Δ0 ura3Δ0*	This study	6E
MTY3525	*rpn4Δ::kanMX6 his3Δ1 leu2Δ0 lys2Δ0 ura3Δ0*	Lab stock	6A-C, 6E

753

754 Table S2. *Plasmids used in the present study*

Name	Structure	Source	Purpose
MTP3091	pESC-Leu-GFP-Ubc9-ts	Judith Frydman (pJF1089)	Fig. 5C
MTP3088	p426 103Q GAL	Addgene (cat.# 1188)	Fig. S7
MTP3108	pYES2-α-synuclein-GFP	H. Takagi (Wijayanti et al., 2015)	Fig. 6A-D
MTP3090	pYES2-GFP	K. Ohashi	Fig. 6A

755 Captions for supplementary movies

756 **Movie S1**

757 Time-lapse imaging of QUEEN in *snf1*Δ*adk1*Δ cells in the 2% glucose medium.
758 Corresponding to the data shown in Fig. 3A. The QUEEN ratio decreased twice (116 and 132
759 min) within a short interval. White scale bar = 5 μm.

760

761 **Movie S2**

762 Another example of *snf1*Δ*adk1*Δ cells showing a sudden decrease in the QUEEN ratio.
763 Corresponding to the data shown in Fig. 3B. The QUEEN ratio decreased twice (180 and 356
764 min) with a long interval. White scale bar = 5 μm.

765

766 **Movie S3**

767 Oscillatory behavior of the QUEEN ratio in *bas1*Δ cells. Corresponding to the data shown in
768 Fig. 3E. Left, the QUEEN ratio image; middle, Myo1-mCherry (inverted grayscale image);
769 right, bright field image. Images were taken every 4 min. White scale bar = 5 μm.

770

771 **Movie S4**

772 Another example of *bas1*Δ cells showing an oscillating QUEEN ratio. Corresponding to the
773 data shown in Supplementary Fig. S4A. Left, the QUEEN ratio image; right, bright field
774 image. In this case, cytokinesis had already been completed at t = 0 min. Images were taken
775 every 3 min. White scale bar = 5 μm.

776

777

Fig. 1

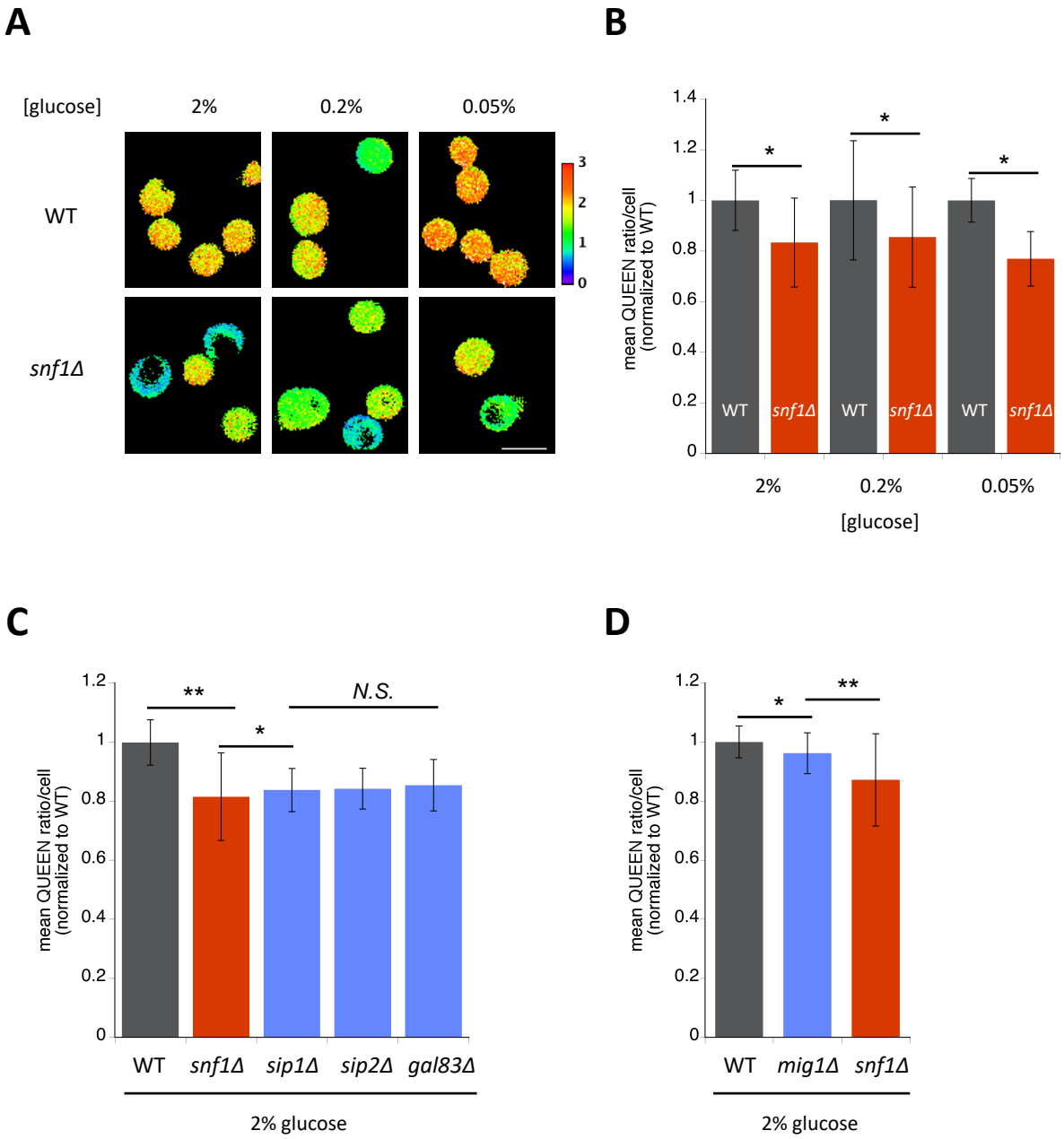
A
[glucose]
2%
0.2%
0.05%
WT
snf1Δ
3
2
1
0
B
mean QUEEN ratio/cell (normalized to WT)
1.4
1.2
1
0.8
0.6
0.4
0.2
0
*
*
*
WT
snf1Δ
WT
snf1Δ
WT
snf1Δ
2%
0.2%
0.05%
[glucose]
C
mean QUEEN ratio/cell (normalized to WT)
1.2
1
0.8
0.6
0.4
0.2
0
**
*
N.S.
WT
snf1Δ
sip1Δ
sip2Δ
gal83Δ
2% glucose
D
mean QUEEN ratio/cell (normalized to WT)
1.2
1
0.8
0.6
0.4
0.2
0
*
**
WT
mig1Δ
snf1Δ
2% glucose

Fig. 2

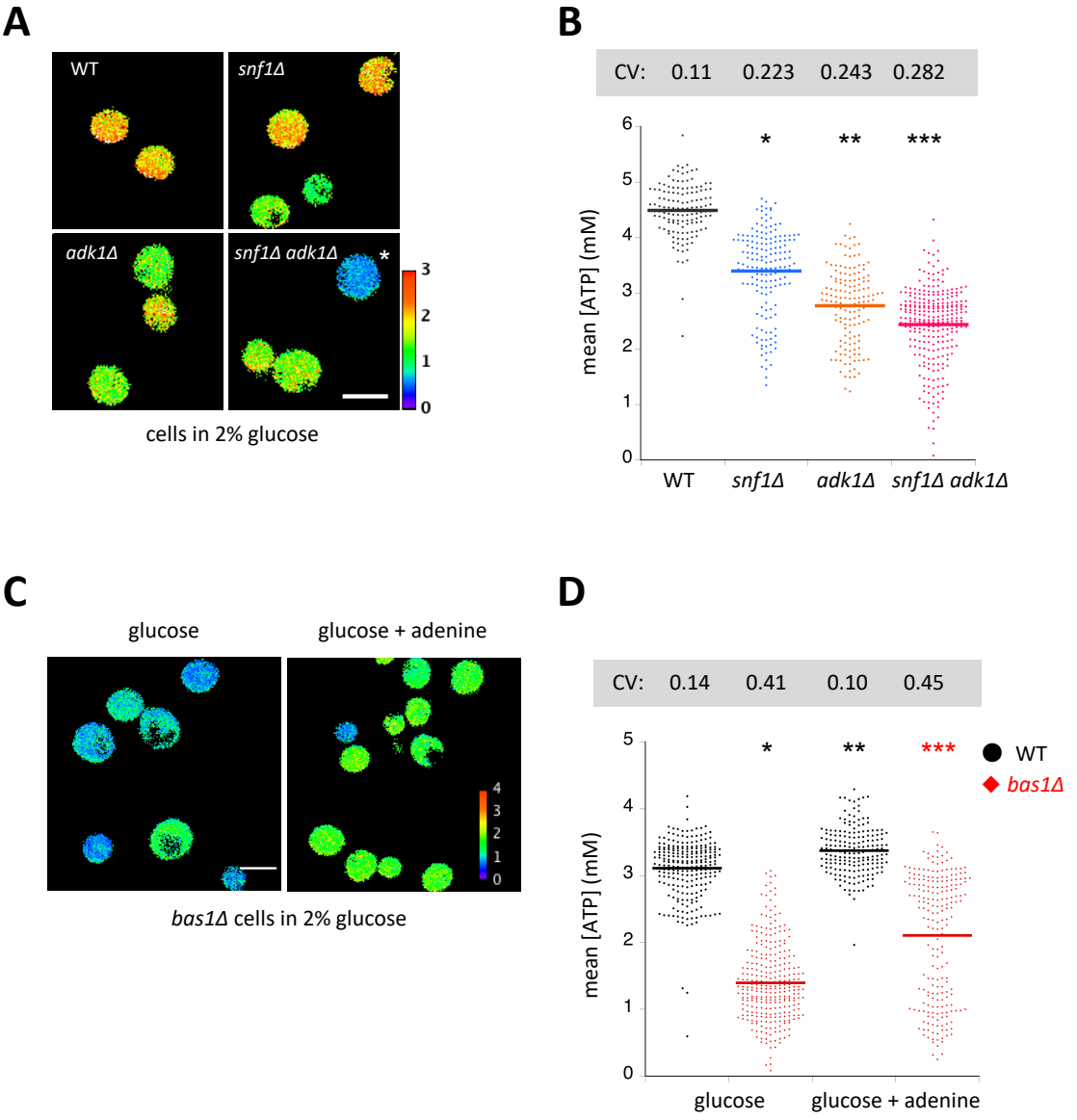
A
WT
snf1Δ
adk1Δ
snf1Δ adk1Δ
*
3
2
1
0
cells in 2% glucose
B
CV: 0.11 0.223 0.243 0.282
mean [ATP] (mM)
6
5
4
3
2
1
0
*
**
***
WT
snf1Δ
adk1Δ
snf1Δ adk1Δ
C
glucose
glucose + adenine
4
3
2
1
0
bas1Δ cells in 2% glucose
D
CV: 0.14 0.41 0.10 0.45
mean [ATP] (mM)
5
4
3
2
1
0
*
**
***
WT
bas1Δ
glucose
glucose + adenine

Fig. 3

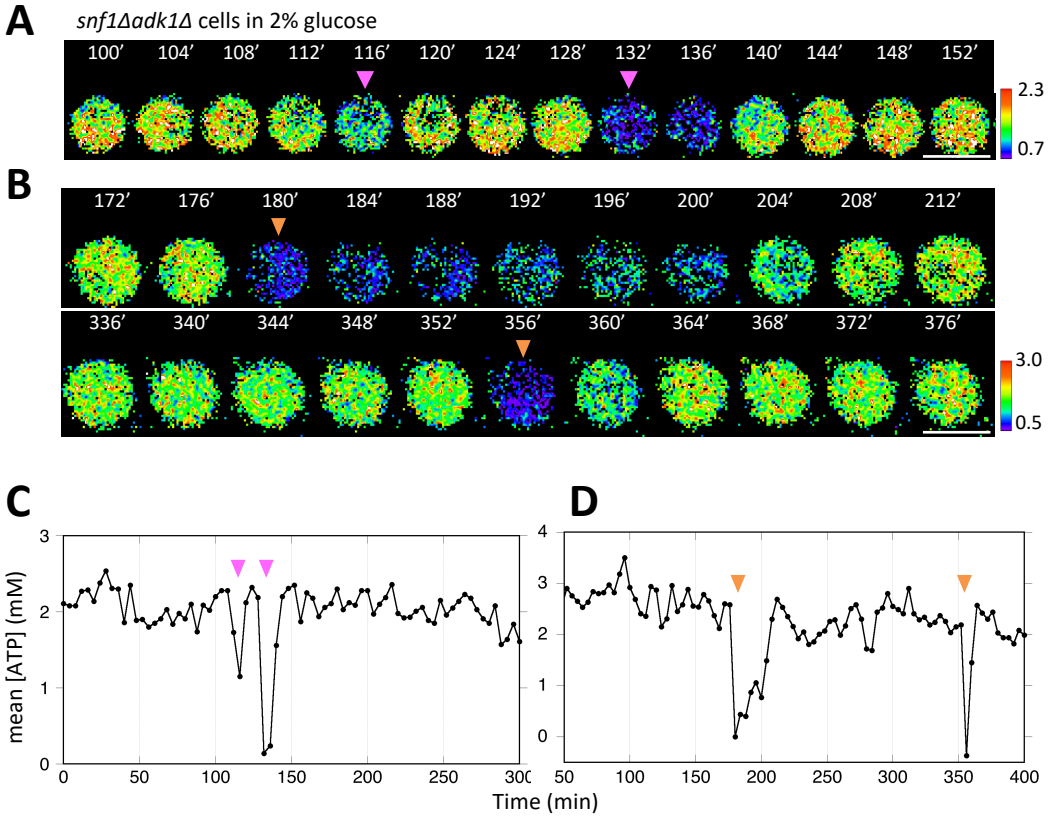
A
snf1Δadk1Δ cells in 2% glucose
100′ 104′ 108′ 112′ 116′ 120′ 124′ 128′ 132′ 136′ 140′ 144′ 148′ 152′
2.3
0.7
B
172′ 176′ 180′ 184′ 188′ 192′ 196′ 200′ 204′ 208′ 212′
336′ 340′ 344′ 348′ 352′ 356′ 360′ 364′ 368′ 372′ 376′
3.0
0.5
C
D
mean [ATP] (mM)
Time (min)

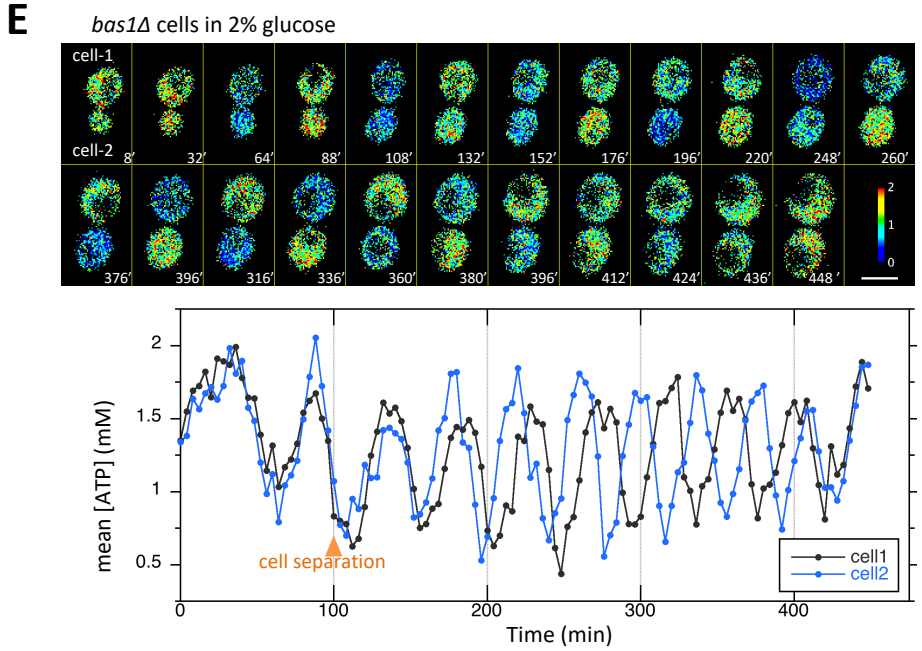
E
bas1Δ cells in 2% glucose
cell-1
cell-2
8′ 32′ 64′ 88′ 108′ 132′ 152′ 176′ 196′ 220′ 248′ 260′
376′ 396′ 316′ 336′ 360′ 380′ 396′ 412′ 424′ 436′ 448′
mean [ATP] (mM)
cell separation
cell1
cell2
Time (min)

Fig. 4

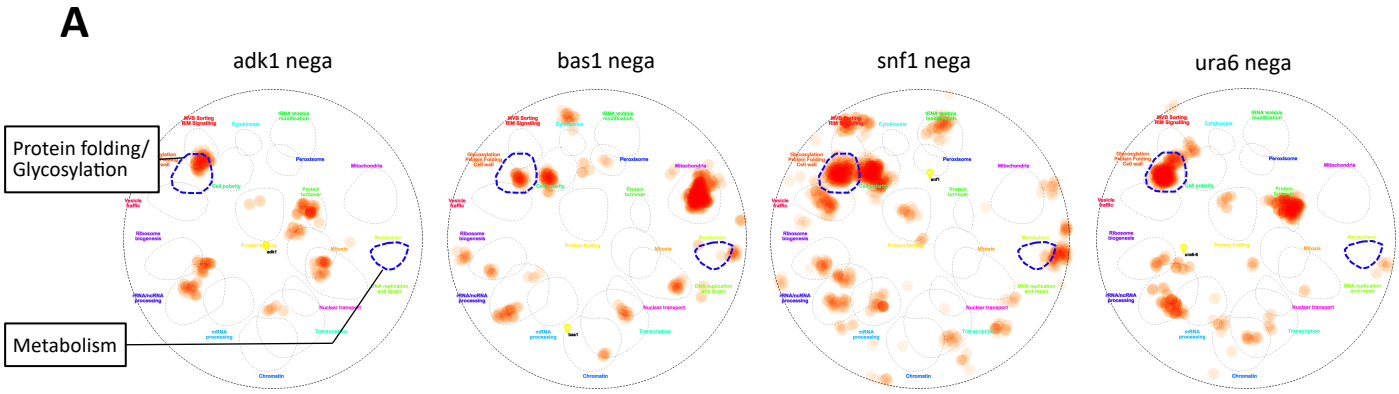
A
adk1 nega
bas1 nega
snf1 nega
ura6 nega
Protein folding/
Glycosylation
Metabolism

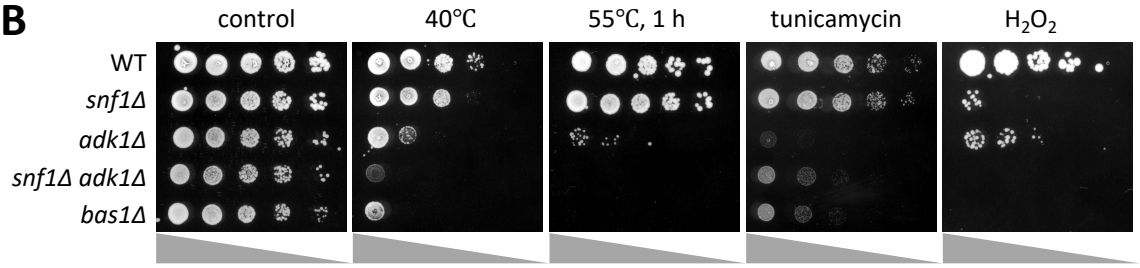
B
control
40°C
55°C, 1 h
tunicamycin
H_2O_2
WT
snf1Δ
adk1Δ
snf1Δ adk1Δ
bas1Δ

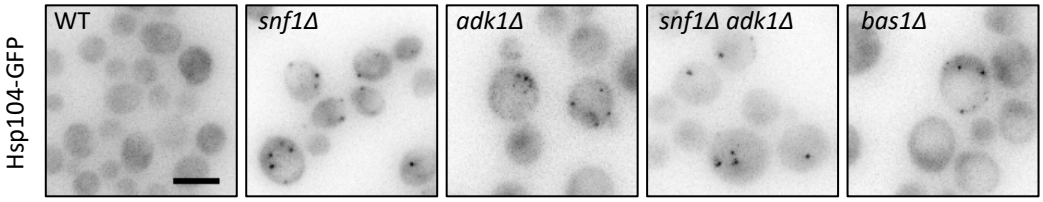
C
Hsp104-GFP
WT
snf1Δ
adk1Δ
snf1Δ adk1Δ
bas1Δ

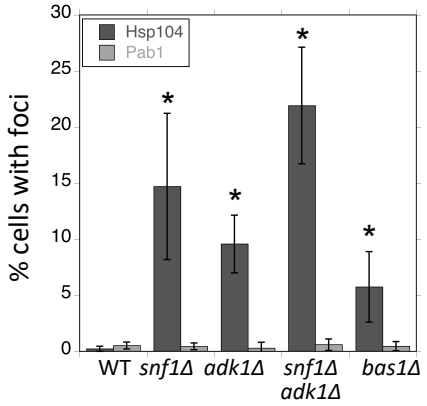
D
% cells with foci
Hsp104
Pab1
0
5
10
15
20
25
30
*
WT
snf1Δ
adk1Δ
snf1Δ adk1Δ
bas1Δ

Fig. 5

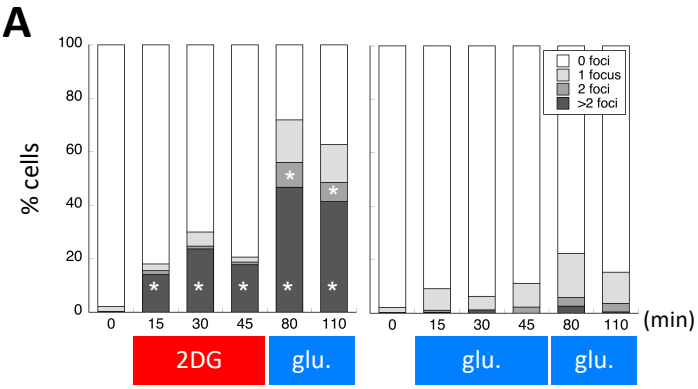
A
% cells
100
80
60
40
20
0
0 foci
1 focus
2 foci
>2 foci
0
15
30
45
80
110
(min)
2DG
glu.
glu.
glu.

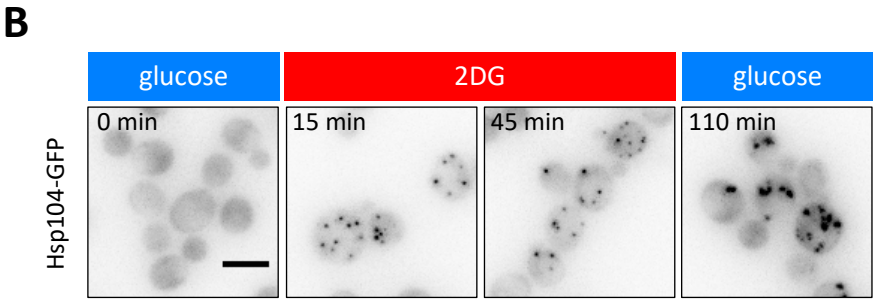
B
glucose
2DG
glucose
Hsp104-GFP
0 min
15 min
45 min
110 min

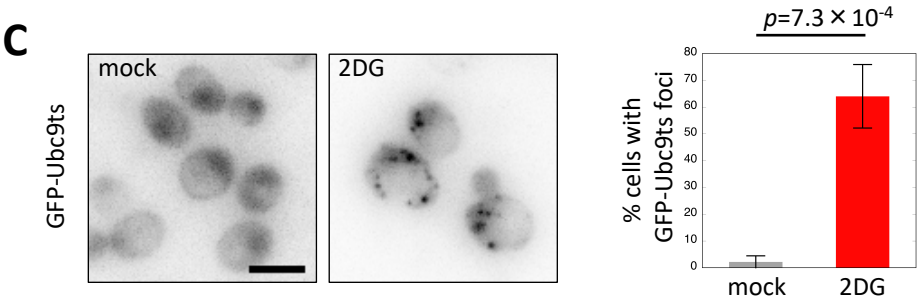
C
GFP-Ubc9ts
mock
2DG
p=7.3 × 10-4
% cells with GFP-Ubc9ts foci
80
70
60
50
40
30
20
10
0
mock
2DG

Fig. 6

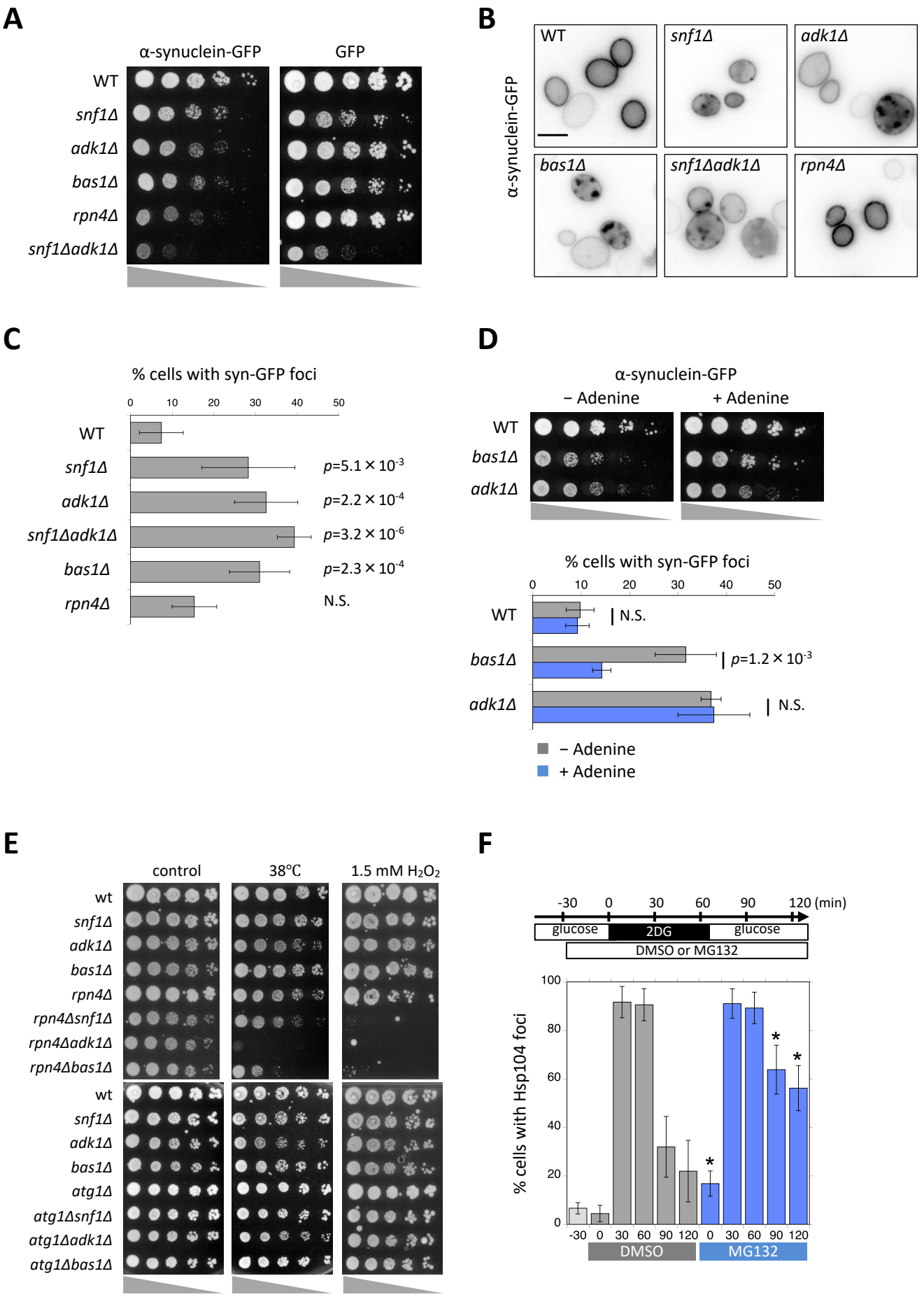
A
α-synuclein-GFP
GFP
WT
snf1Δ
adk1Δ
bas1Δ
rpn4Δ
snf1Δadk1Δ
B
α-synuclein-GFP
WT
snf1Δ
adk1Δ
bas1Δ
snf1Δadk1Δ
rpn4Δ
C
% cells with syn-GFP foci
0
10
20
30
40
50
WT
snf1Δ
adk1Δ
snf1Δadk1Δ
bas1Δ
rpn4Δ
p=5.1 × 10-3
p=2.2 × 10-4
p=3.2 × 10-6
p=2.3 × 10-4
N.S.
D
α-synuclein-GFP
− Adenine
+ Adenine
WT
bas1Δ
adk1Δ
% cells with syn-GFP foci
0
10
20
30
40
50
WT
N.S.
bas1Δ
p=1.2 × 10-3
adk1Δ
N.S.
− Adenine
+ Adenine
E
control
38°C
1.5 mM H2O2
wt
snf1Δ
adk1Δ
bas1Δ
rpn4Δ
rpn4Δsnf1Δ
rpn4Δadk1Δ
rpn4Δbas1Δ
wt
snf1Δ
adk1Δ
bas1Δ
atg1Δ
atg1Δsnf1Δ
atg1Δadk1Δ
atg1Δbas1Δ
F
-30
0
30
60
90
120 (min)
glucose
2DG
glucose
DMSO or MG132
% cells with Hsp104 foci
100
80
60
40
20
0
-30 0 30 60 90 120 0 30 60 90 120
DMSO
MG132

Fig. 7

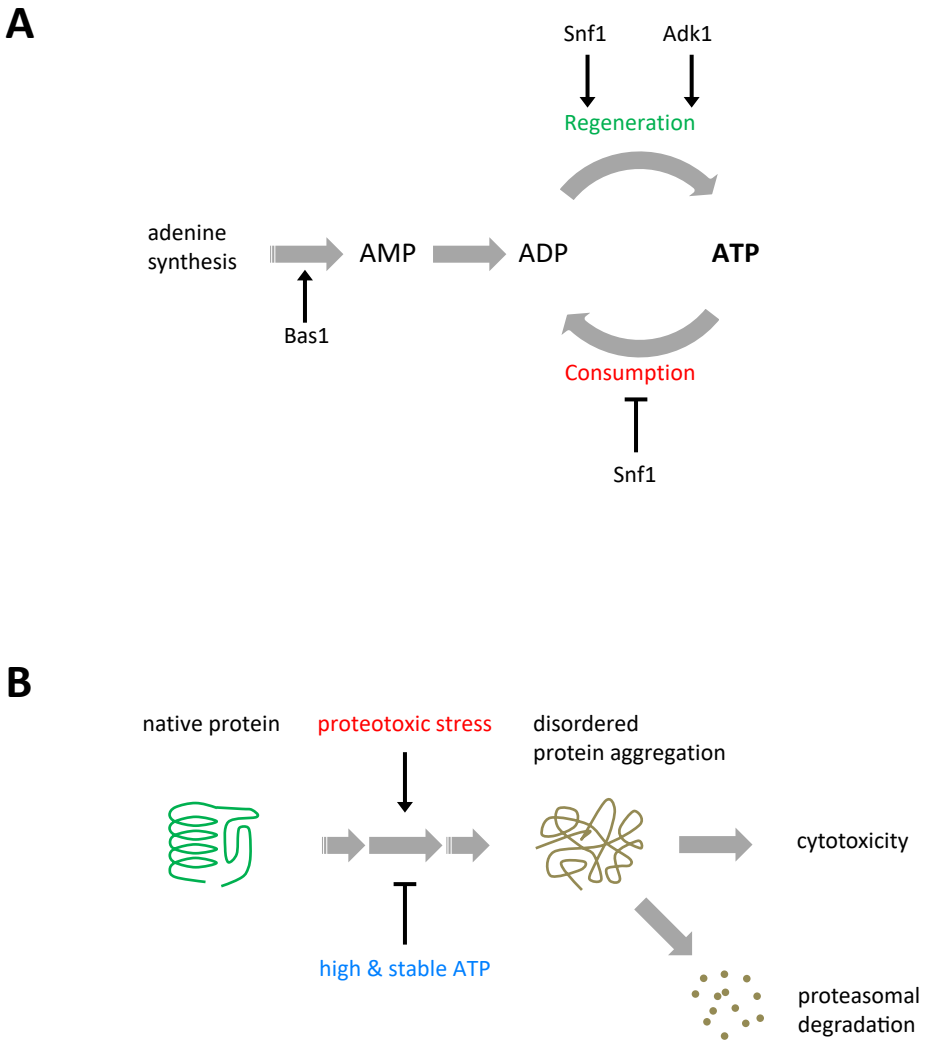
A
Snf1
Adk1
Regeneration
adenine
synthesis
AMP
ADP
ATP
Bas1
Consumption
Snf1
B
native protein
proteotoxic stress
disordered
protein aggregation
cytotoxicity
high & stable ATP
proteasomal
degradation

Fig. S1

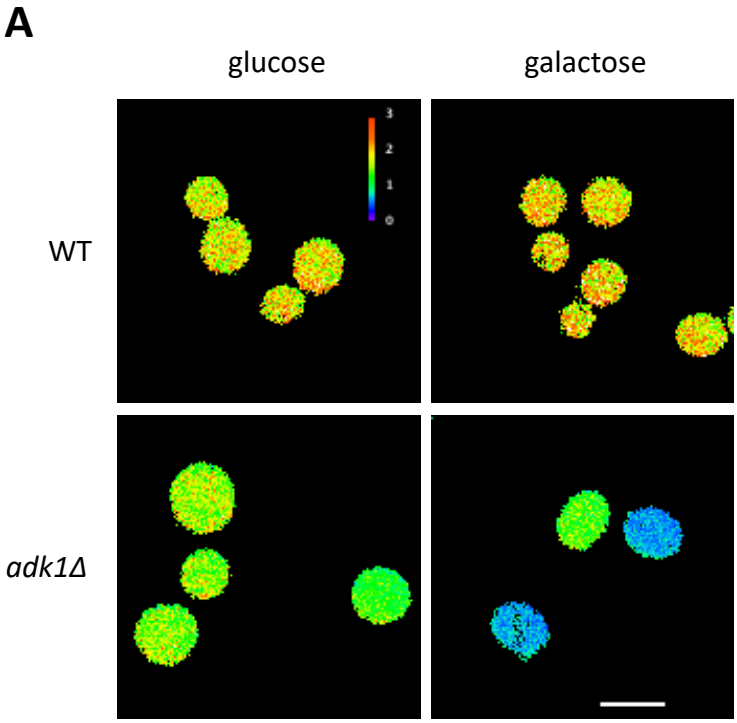
A
glucose
galactose
WT
adk1Δ
3
2
1
0

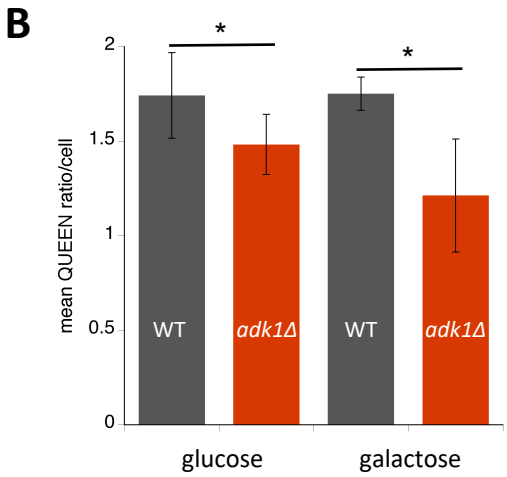
B
mean QUEEN ratio/cell
2
1.5
1
0.5
0
*
*
WT
adk1Δ
WT
adk1Δ
glucose
galactose

Fig. S2

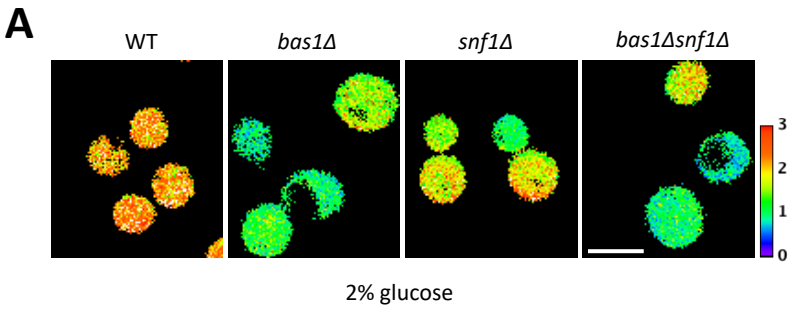
A
WT
bas1Δ
snf1Δ
bas1Δsnf1Δ
3
2
1
0
2% glucose

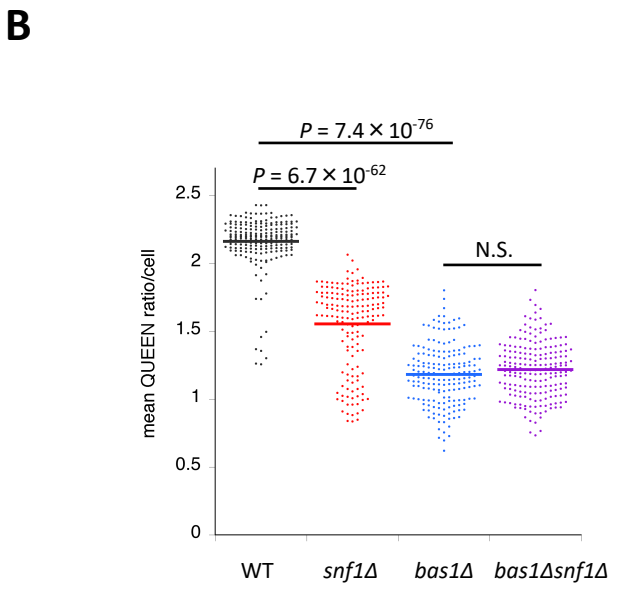
B
P = 7.4 × 10-76
P = 6.7 × 10-62
N.S.
mean QUEEN ratio/cell
2.5
2
1.5
1
0.5
0
WT
snf1Δ
bas1Δ
bas1Δsnf1Δ

Fig. S3

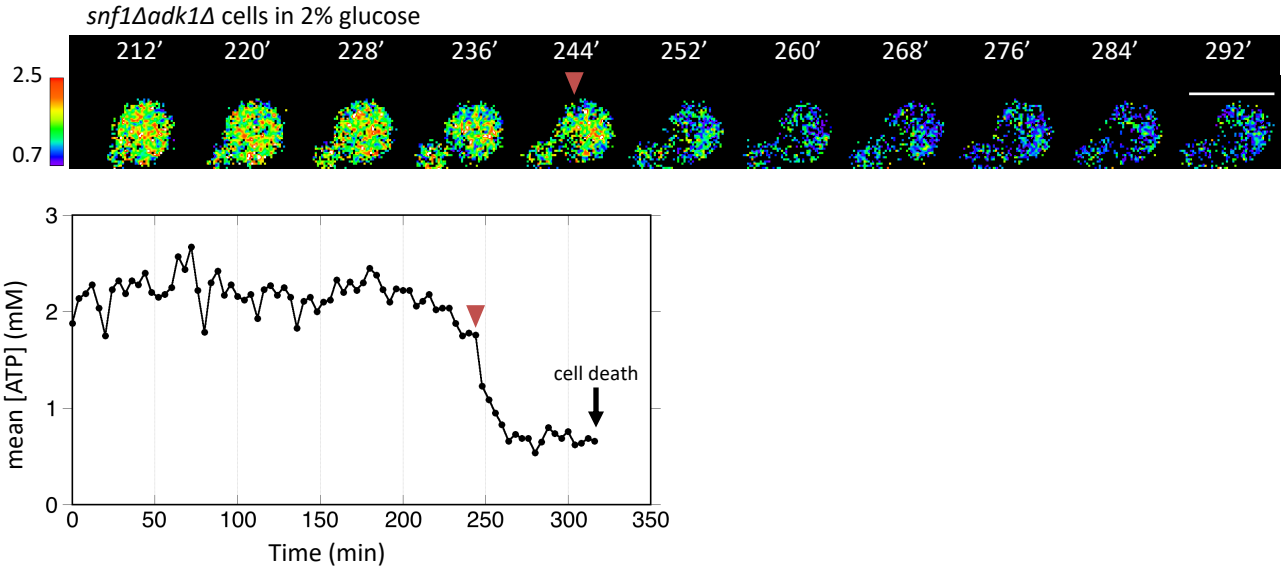
snf1Δadk1Δ cells in 2% glucose
212’
220’
228’
236’
244’
252’
260’
268’
276’
284’
292’
2.5
0.7
mean [ATP] (mM)
3
2
1
0
0
50
100
150
200
250
300
350
Time (min)
cell death

Fig. S4

A

bas1Δ cells in 2% glucose

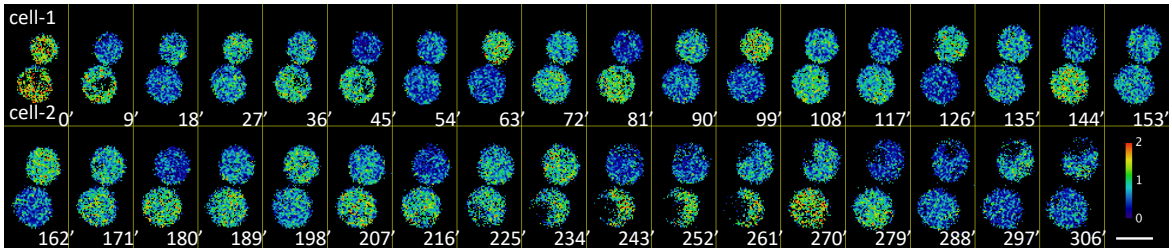

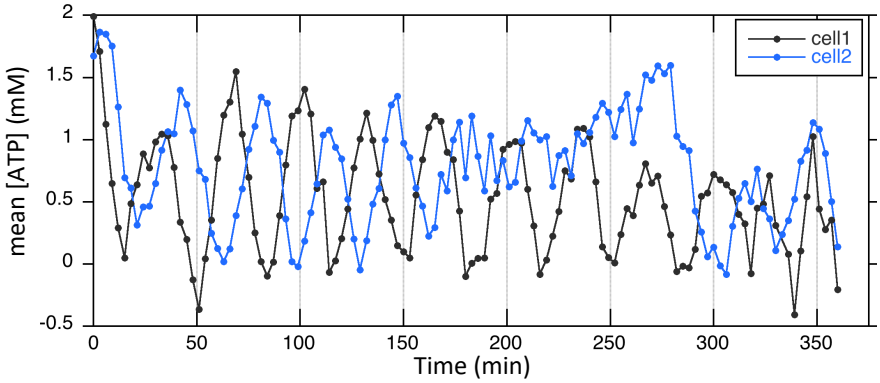

B

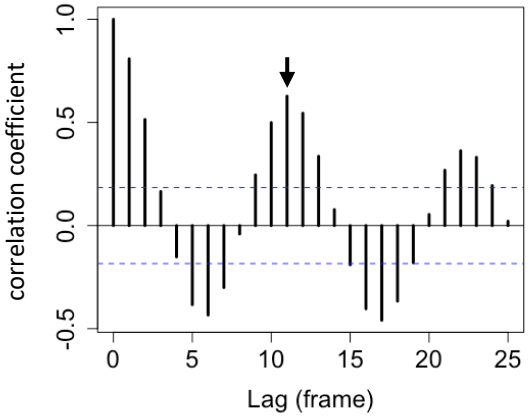

Fig. S5

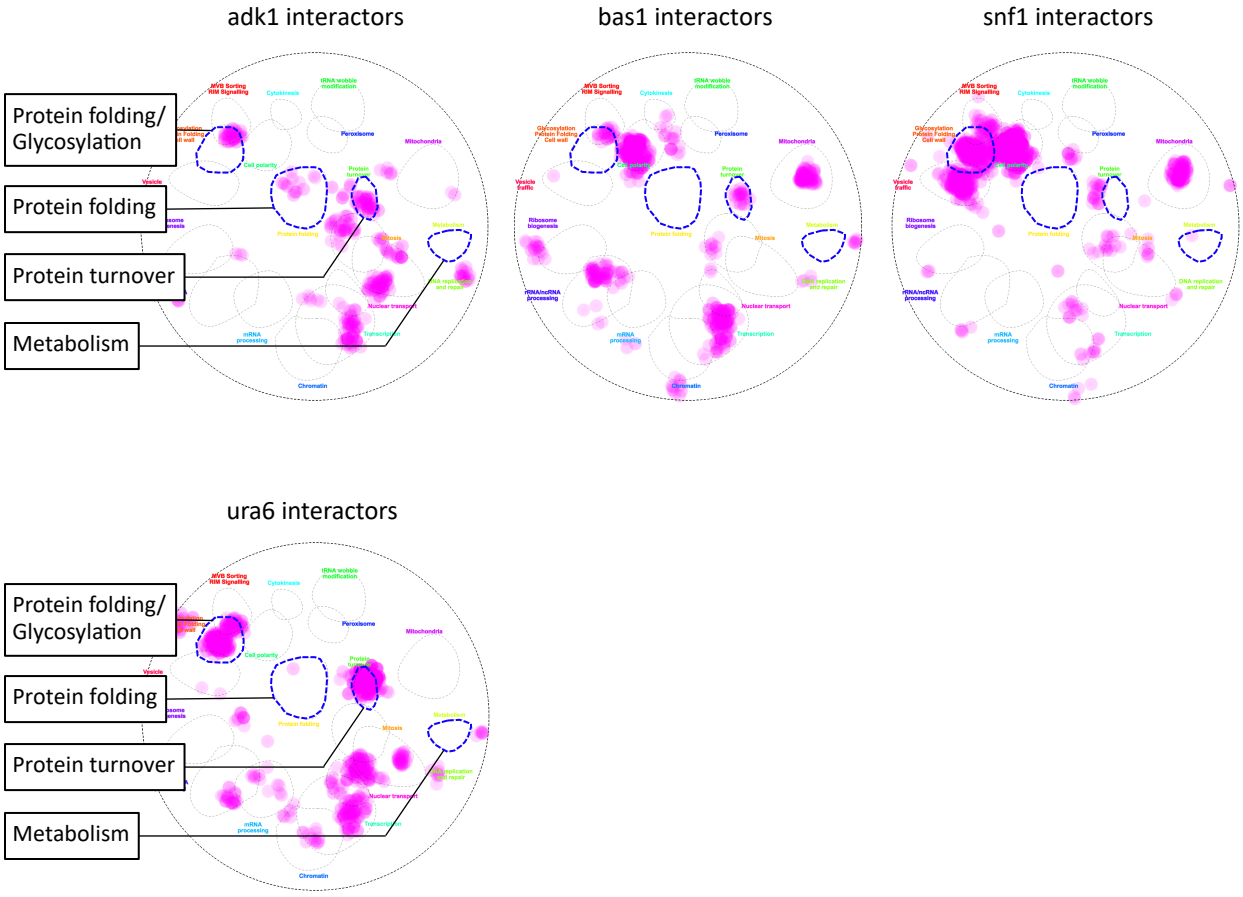
adk1 interactors
bas1 interactors
snf1 interactors
ura6 interactors
Protein folding/ Glycosylation
Protein folding
Protein turnover
Metabolism

Fig. S6

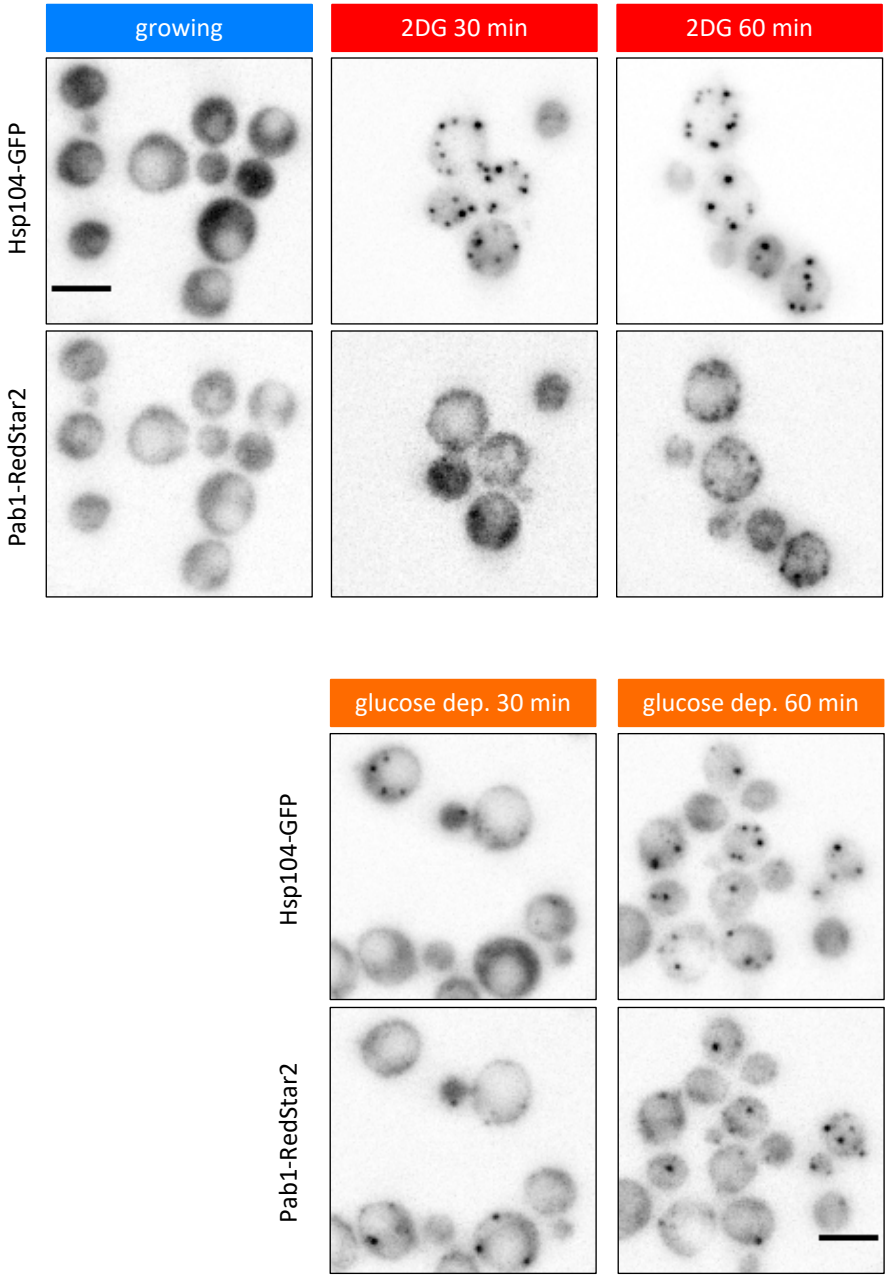
growing
2DG 30 min
2DG 60 min
Hsp104-GFP
Pab1-RedStar2
glucose dep. 30 min
glucose dep. 60 min
Hsp104-GFP
Pab1-RedStar2
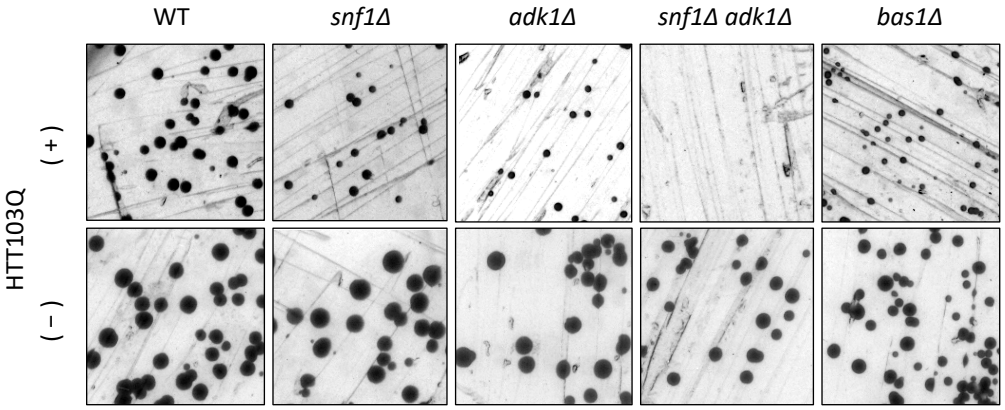
Fig. S7